Non-Planar Reinforced Concrete Walls: Assessing Effective Stiffness and Influence of Axial Load Ratio and Eccentricity with Simplified Beam-Truss Models

João Pacheco de Almeida [a], Basile Payen [a], Ryan Hoult [a]*, and António A. Correia [b]

[a] Institute of Mechanics, Materials and Civil Engineering, UCLouvain, Louvain-la-Neuve, Belgium.
E-mail: joao.almeida@uclouvain.be

[b] LNEC, National Laboratory for Civil Engineering, Lisbon, Portugal.

* Present address: School of Engineering, University of Newcastle, Australia.

Keywords: *Non-planar walls, Effective stiffness, Axial load ratio, Axial load eccentricity, Beam-truss models, Reinforced concrete.*

Abstract

This study investigates the effective stiffness of non-planar reinforced concrete walls, a key parameter in seismic design. By assembling a database of experimental cyclic tests, it highlights how effective stiffness varies with wall geometry, loading direction, and axial load ratio and eccentricity – factors often neglected in current code formulations. Using pushover analyses with a simplified beam-truss model (BTM), the study demonstrates good agreement with experimental data and supports BTM use for estimating effective stiffness. The findings underscore the need to revise effective stiffness definitions in design codes and promote further research for better seismic design of non-planar walls.

1 Introduction

Most medium-to-high-rise buildings worldwide are reinforced concrete (RC) structures; they generally use structural walls as lateral load resisting systems, which dominantly control the overall seismic and wind response. The number of RC walls per building and their cross-sectional shapes vary significantly as a function of geographical location, seismicity, national or regional design and construction practices, among other factors. This diversity was recently observed in surveillance work on RC buildings following the destructive Turkish earthquake of February 6, 2023 (Kazaz 2024; Vuran et al. 2024). Namely, core walls are often U-shaped, H-shaped, or E-shaped, and many other structural walls in buildings also take non-planar forms, e.g. T-shaped or L-shaped. These observations are at odds with the fact that most past experimental research on RC walls, design methods, and nonlinear modelling techniques focused on planar walls. The current investigation is a contribution to a key aspect of non-planar RC wall seismic design and assessment, namely their effective stiffness. As explained below, it builds on the validation and application of an accurate yet practice-compatible modelling approach, the so-called beam-truss models (Miki and Niwa 2004).

Seismic design and assessment of buildings involve, as a minimum, the application of a static lateral force method or/and response spectrum method of analysis, which are familiar to all seismic design engineers. They both employ a linear analysis that implicitly accounts for overstrength and nonlinear response through a behaviour or strength reduction factor; verifications are performed in terms of forces, reason for which they are sometimes called "force-based" (FB) approaches. A simplified idealisation of the behaviour of RC members such that they can be modelled using a linear-elastic analysis approach is crucial for the engineer's ability to design structures. Reasonable estimates of the seismic demand, not only in terms of forces but also for displacement verifications, require an adequate choice for the stiffness of the structural elements, connected to a numerical model and a representative behaviour factor. The so-called effective stiffness considers the fact that, during ground motion shaking, RC walls will crack over a significant region, and the reinforcement will yield in some locations, namely at the base of the walls. An appropriate estimation of the effective stiffness of RC walls, K_{eff}, is vital as it governs the lateral stiffness of the whole structural system, with potential significant effects for the entire structural design and assessment. The effective stiffness of members is typically defined as a proportion of the initial uncracked stiffness K_g. Since beams, columns, and walls were, historically and in many cases still today, modelled with beam elements, such stiffness modifiers are generally expressed as a ratio of the gross cross-section moment of inertia I_g, i.e. as ratios I_{eff} / I_g, on the consideration that $K_{eff} / K_g = I_{eff} / I_g$. Depending on the specific proposal, these ratios can be a function of several variables, e.g. the axial load ratio. A review of existing expressions, both in the literature and in the codes, is performed in Section 2.1, which this study will later show to present fundamental limitations for non-planar walls.

Today, advanced models for simulating the nonlinear seismic response of structures are available to design engineers, being accessible both in terms of complexity and alignment with project schedules. They allow for increasingly accurate estimates of structural deformation demands using nonlinear static or dynamic analyses, which can then be compared – either at the global (structural) level or at the local (member) level – with the corresponding capacities. This forms the basis of the so-called "displacement-based" (DB) approaches, which are in principle more accurate than FB ones since they employ refined models to simulate the nonlinear response of the entire structure. Unsurprisingly, DB methods are progressively being allowed not only for structural assessment but also for the design of new structures; for example, this is one of the key changes included in the soon-to-be-released second generation of Eurocode 8 (CEN 2024), with respect to the current generation (CEN 2004a).

Recent studies have shown that an unsatisfactory determination of the effective stiffness of vertical members is the basis for discrepancies between FB and DB approaches (Almeida et al. 2022). The minimization of such disparities can be attained by the employment of stiffness modifiers, in linear-elastic models for FB approaches, that are compatible with the nonlinear models required for the static and dynamic analyses used in DB methods. The harmonisation of models for DB and FB approaches is all the more pressing since, in the context of design of new buildings, DB methods still require a FB approach for preliminary structural design. It is noted, however, that current and future codes (e.g. the next-generation Eurocode 8) progressively cast DB methods as alternative – and not just supplementary – approaches to design and assessment, with respect to FB ones.

Among a host of modelling approaches for non-planar walls, which are briefly reviewed in Section 3.1, the so-called nonlinear Beam-Truss Models (BTMs) have shown to deliver a remarkable compromise between conceptual clarity, ease of implementation in engineering practice, accuracy, and computational time. BTMs have been validated against experimental results of rectangular walls (Deng et al. 2021) and non-planar walls loaded quasi-statically along one or both horizontal axes (Lu and Panagiotou 2014), or about the vertical axis (Hoult et al. 2023b; Mavros et al. 2026). Recently, they have also found their way into full building dynamic response simulation (Mavros et al. 2022; Zhang et al. 2017). The current work revises the body of literature relative to BTMs and presents an extensive application of a simplified and standardized BTM to simulate the test results of 12 non-planar walls; particular focus is given to the model's ability to acceptably simulating the nonlinear force-displacement monotonic envelope of the cyclic response, and the corresponding effective stiffness. Both push and pull directions will be considered for the pushover of walls with asymmetric sections. The accuracy of the experimental *vs* simulated effective stiffness will then be assessed and compared with expressions in the literature and design codes.

An important variable addressed in the current investigation is the influence of gravity-induced axial load on the response of non-planar walls, a topic that has received limited attention to date, in particular regarding two aspects: (i) the influence of the axial load ratio on the effective stiffness, and the extent to which existing code and literature formulations manage or fail to capture it; (ii) the effects of the eccentricity of the resultant axial force on the wall nonlinear behaviour. As far as the authors are aware, this latter point has been insufficiently explored in the literature and is not usually considered in design practice. In engineering applications, linear-elastic models for FB design and assessment typically represent non-planar walls using beam elements defined at the member's center of gravity, wide-column models (Beyer et al. 2008a), other frame-equivalent approaches such as BTMs, or shell elements. However, there is currently limited guidance on appropriate stiffness modifiers to account for the effects of axial load eccentricity – which is generally unavoidable – on wall response, nor on methods to quantify them. This issue is examined in Section 5.3, where validated nonlinear BTMs are used to estimate the influence of axial load eccentricity on effective stiffness. Section 5.2. addresses, with the same simulation approach, the impact of the axial load ratio on non-planar wall effective stiffness.

2 Effective Stiffness of Non-planar Walls and Experimental Database

2.1 Literature review, code values, and formulations for non-planar sections

The direct and fundamental role of RC walls' effective stiffness K_{eff} in the estimation of seismic forces for both structural design and assessment has led to thorough discussions and research over the past decades. Some of the main contributions are quickly reviewed herein. Beforehand, it is recalled that the effective stiffness K_{eff} is often, alternatively, described in terms of the effective moment of inertia I_{eff}. The latter usually holds most meaning for design engineers, when members are modelled as line elements, since it is typically the required input parameter for defining the cross-section parameters in the model. It is common to express K_{eff} and I_{eff} in terms of their gross counterparts, K_g and I_g, i.e. through an effective stiffness ratio K_{eff} / K_g or I_{eff} / I_g.

summarises recommendations for the effective stiffness as indicated in some of the most relevant international codes, which the regulations allow to be used unless more refined analyses are performed. In particular, the table includes the current (CEN 2004a) and next generation (CEN 2024) Eurocode 8, the American codes ACI 318-9 (American Concrete Institute 2019) and ASCE/SEI 41-17 (American Society of Civil Engineers 2017), and the New Zealand Standard (2006). It is believed that the proposed code expressions were developed for planar walls, as the ACI 318-19 (American Concrete Institute 2019) separation in "in-plane" and "out-of-plane" suggests. Other codes, such as the Canadian Standard CSA A23.3, also contain expressions for the effective stiffness derived for use in displacement-based verifications of the top-wall displacement of walls (Adebar and Dezhdar 2015). Additionally, Table 1 shows some well-known proposals from the literature (Fenwick and Bull 2000; Paulay and Priestley 1992). The works by Wibowo et al. (2013) and Wong et al. (2017) include the review of other expressions. The degree to which these expressions have been developed specifically for non-planar walls seems to be either minimal or absent. The work by Priestley et al. (2007a) is also of relevance within the present context in that their research showed that member effective stiffness is related to its strength; consequently, since member strengths are the end product of force-based design, successive iterations should be carried out, with corresponding recalculation of the members' effective stiffnesses (Das and Choudhury 2019). Table 1 excludes proposals for squat structural walls (Li and Xiang 2011), for high-rise buildings (Adebar et al. 2007; Rahimian 2011), and other expressions exclusively focused on planar walls (Sharifi and Shafieian 2018).

Table 1. Some existing proposals for the effective moment of inertia for RC walls (squat walls excluded).

Reference		**Effective Stiffness, I_{eff}**	
Eurocode 8: current (CEN 2004a) and next generation (CEN 2024)		$0.5I_g$	
ACI 318-19	In-plane	$0.35I_g$	
	Out-of-plane	$0.25I_g$	
ASCE/SEI 41-17 (Table 10-5)		$0.35I_g$	
NZS 3101:Part 2:2006	Ultimate limit state	$N/(A_g f_c') = 0.2$	For $f_y = 300\ MPa$: $0.48I_g$
			For $f_y = 500\ MPa$: $0.42I_g$
		$N/(A_g f_c') = 0.1$	For $f_y = 300\ MPa$: $0.40I_g$
			For $f_y = 500\ MPa$: $0.33I_g$
		$N/(A_g f_c') = 0.0$	For $f_y = 300\ MPa$: $0.32I_g$
			For $f_y = 500\ MPa$: $0.25I_g$
	Serviceability limit state	$\mu = 1.25$	I_g
		$\mu = 3$	$0.7I_g - 0.6I_g - 0.5I_g$ for $N/(A_g f_c') = 0.2 - 0.1 - 0.0$ respectively
		$\mu = 6$	As for ultimate limit states
Paulay and Priestley (1992)	Flexure-dominated	$\left(\frac{100}{f_y} + \frac{N}{f_c' A_g}\right) I_g$	
	Shear-dominated	$\frac{\left(\frac{100}{f_y} + \frac{N}{f_c' A_g}\right) I_g}{1.2 + C}$, where $C = \frac{30\left(\frac{100}{f_y} + \frac{N}{f_c' A_g}\right) I_g}{H_w^2 t_w L_w}$	
Fenwick and Bull (2000)		$0.267\left(1 + 4.4\frac{N}{f_c' A_g}\right)\left(0.62 + \frac{190}{f_y}\right)(0.76 + 0.005 f_c') I_g$	
For non-planar walls: Zhang and Li (2018)		T-shaped, flange in tension	$\frac{1}{1 + \frac{40 I_f}{H_w^2 b_w l_w}} I_f$, where $I_f = \left(2.35\frac{N}{f_c' A_g} + \frac{185}{f_y}\right) I_g$
		T-shaped, flange in compression	$\frac{1}{1 + \frac{30 I_f}{H_w^2 b_w l_w}} I_f$, where $I_f = \left(1.75\frac{N}{f_c' A_g} + \frac{125}{f_y}\right) I_g$
		U-shaped, strong axis	$\frac{1}{1 + \frac{40 I_f}{H_w^2 b_w l_w}} I_f$, where $I_f = \left(1.82\frac{N}{f_c' A_g} + \frac{60}{f_y}\right) I_g$
		U-shaped, flange in compression	$\frac{1}{1 + \frac{40 I_f}{H_w^2 b_w l_w}} I_f$, where $I_f = \left(1.85\frac{N}{f_c' A_g} + \frac{180}{f_y}\right) I_g$
		U-shaped, flange in tension	$\frac{1}{1 + \frac{40 I_f}{H_w^2 b_w l_w}} I_f$, where $I_f = \left(3.02\frac{N}{f_c' A_g} + \frac{183}{f_y}\right) I_g$

Nomenclature. I_g: gross moment of inertia; A_g: gross-sectional area of the wall; f_c': concrete compressive strength; *N*: axial load (taken positive for compression); f_y: yield strength of longitudinal reinforcement; μ: structural ductility factor; H_w: wall height; b_w: wall thickness; l_w: wall length.

Some factors are recognized, both in the literature and some codes (Fenwick and Bull 2000; New Zealand Standard 2006; Paulay and Priestley 1992), to influence the effective stiffness of planar RC walls: (i) the applied axial load ratio (ALR; the ratio of the applied axial load *N* to the compressive load capacity of the element, $A_g f_c'$, where A_g corresponds to the gross-sectional area of the wall and f_c' to the concrete compressive strength); (ii) the longitudinal reinforcement yield strength, which influences the curvature at first yield; (iii) for shear-dominated walls: the shear span ratio (SSR), and geometric parameters such as the wall thickness and length. Additional governing factors were suggested in other studies, which analyses have shown not to be relevant or difficult to accommodate in engineering design practice (Fenwick and Bull 2000; New Zealand Standard 2006; Sharifi and Shafieian 2018), including: the reinforcement ratio (in the wall boundary and/or web), the concrete tensile strength and the extent of flexural and shear cracking (which influence the magnitude of tension stiffening), or the conditions in the member before seismic action (e.g. creep and shrinkage can induce compression in the reinforcement). The factors considered to play the major role are included in the expressions in Table 1, namely the axial load ratio and the yield strength of the longitudinal reinforcement. The SSR is not explicitly accounted for in the expressions shown, which can therefore be considered inapplicable to squat walls — typically characterized by an SSR below approximately 1.5, and for which dedicated expressions exist (Li and Xiang 2011). Some expressions in the table also make allowance for anchorage slip at the wall base (Paulay and Priestley 1992).

Finally, Table 1 also includes the expressions proposed by Zhang and Li (2018), based on finite element (FE) analyses; as far as the authors are aware, the latter are the only ones explicitly derived for non-planar walls. Unsurprisingly, the number of factors influencing the effective stiffness of non-planar walls increases with respect to rectangular walls, for at least three additional factors need to be taken into account as indicated by Zhang and Li (2018): (i) the cross-sectional geometry; (ii) the loading axis; (iii) the loading direction. Some other contributions to the effective stiffness of non-planar cross-sections recently started joining the literature, for instance, the study by Samanta and Dasgupta (2024), which among other conclusions show that, for T-shaped walls, the effective stiffness largely depends on specific details of the cross-section shape, namely the thickness of the web tip / boundary element. From the above review, it is apparent that many factors should be considered to correctly estimate the effective stiffness of non-planar walls. This study will also analyse and show the relevance of another variable, namely the axial load eccentricity.

In the scope of the present investigation, the two next distinct definitions or methods to compute the effective stiffness K_{eff} are employed. They are widely accepted in the literature (Fenwick and Bull 2000; Li and Xiang 2011) and can be calculated based on the results of a pushover curve:

- Method 1: The effective stiffness is defined by the slope of the secant to the shear force *vs* lateral displacement curve crossing the point at 75% of the maximum shear force.
- Method 2: The slope of the secant to the shear force vs lateral displacement curve at first yield. The latter is identified by the first tensile yield of longitudinal reinforcement (occurring in the wall outermost longitudinal reinforcement, i.e. under highest tension), or by the cover concrete compression crushing strain of 0.002, whichever occurs at lower drifts. The precise identification of these events, namely the first yielding, is seldom available for experimental test results. This implies that such method will be employed just for the numerical BTM results.

It is noted that not all expressions in Table 1 are based on the same exact definitions above. Some minor differences can be observed, e.g. ASCE/SEI 41-17 (American Society of Civil Engineers 2017) uses an alternative to Method 1, in which the effective lateral stiffness is obtained as the secant stiffness calculated at a base shear force equal to 60% of the effective yield strength of the structure. Researchers agree that the definition associated to Method 2 has a solid theoretical basis if the main concern is the stiffness under cyclic pre-yield conditions (Fenwick and Bull 2000), since the wall crack pattern will have stabilized, tension stiffening decreased, possible compression from shrinkage released, and hence the wall response has become essentially linear.

2.2 Effective stiffness of studied non-planar walls

Many experimental RC member tests have been performed over the last decades; the present study considers a total of 12 non-planar wall units from the literature, which represent a small fraction compared to the number of walls tested with planar cross-sections. The assembled database includes non-planar specimens that were tested either along the major or minor section axis, or those units that, if loaded biaxially, also included loading phases just along one of the two main section axes while the imposed displacement along the perpendicular axis remained null. Further considerations in this respect will be made in Sections 3.4 and 5.4. The database includes various cross-sectional shapes (U-shaped, rectangular barbell-shaped, T-shaped, and I-shaped) and loadings: (i) UW1: a U-shaped wall cyclically loaded along its minor axis, tested by Hoult et al. (2023c); in Section 3.3 this wall is used as an illustrative example on how the BTM simulation was implemented for all units; (ii and iii) TUA and TUB: two U-shaped walls investigated by Beyer et al. (2008b), subjected to loading parallel to the flanges, the web, and along diagonal directions; (iv) TUE: a slender U-shaped wall analysed by Hoult et al. (2020) with a single layer of vertical reinforcement instead of the standard two layers, also loaded along its two main axes and diagonally; (v, vi, and vii) Wall1, Wall2, and Wall3: two identical U-shaped units tested by Ile and Reynouard (2005) that were subjected to loading about the major (Wall1) and minor axis (Wall2); a third identical wall (Wall3) was tested biaxially following a cloverleaf pattern, which will be further analysed in Section 3.4; (viii and ix) Unit 1.0 and Unit 2.0: two planar walls tested in-plane by Mestyanek (1986) with a non-planar barbell cross-section; it is noted, as further discussed below, that Unit 1.0 is a squat wall, and Unit 2.0 can be classified as an intermediate wall; this will allow to discuss and identify limits on the ability of the adopted BTM to reproduce the experimentally measured effective stiffness; (x) TW2: a T-shaped wall tested by Thomsen IV and Wallace (1995), subjected to cyclic loading along its major axis; (xi) NTW1: a T-shaped wall loaded along both axes (Brueggen 2009; Brueggen et al. 2017); (xii) F1: an I-shaped wall loaded experimentally along its major bending axis by Oesterle et al. (1976). The ALR and the shear span ratio (SSR) of the above-indicated units are indicated in the corresponding graphs of Figure 7. The cross-sections of some of the abovementioned units that will be analysed in more detail in Sections 3.3 and 3.4, or used for sensitivity analyses in Sections 5.2 and 5.3, are represented in Figure 1.

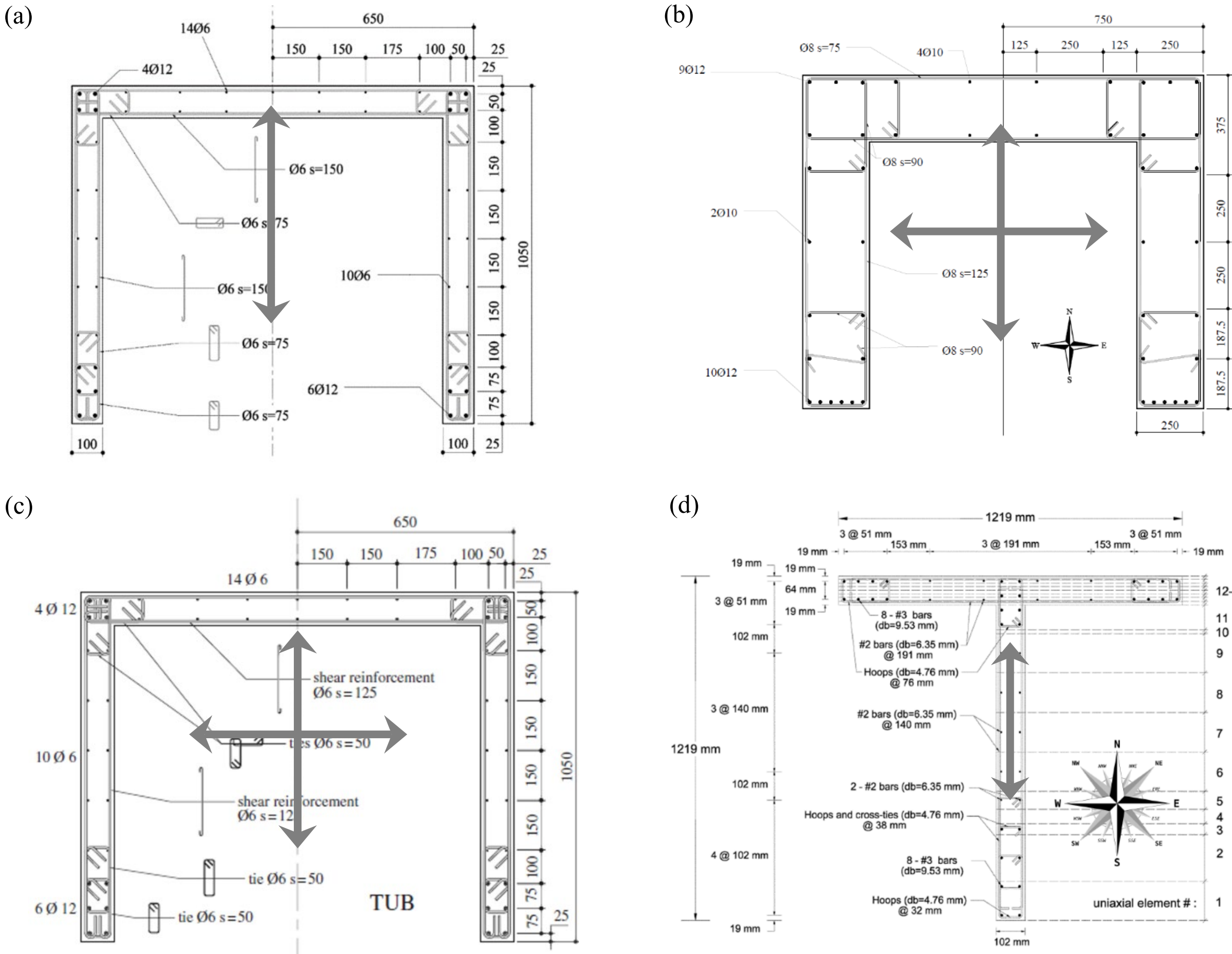

Figure 1. Cross-sections of some of the tested non-planar RC walls considered in the present study, together with analysed loading directions: (a) UW1; (b) Wall3; (c) TUB; (d) TW2.

The following sets of non-planar walls, whose results are available in the literature, were not considered: (i) squat walls – apart from Unit 1.0 by Mestyanek (1986), namely the experimental programmes consisting in a series of H-shaped (Ma and Li 2018), T-shaped (Ma et al. 2018), and L-shaped (Ma and Li 2019) units; (ii) U-shaped walls loaded solely along the diagonal directions, namely the units TUC, TUD, and TUF (Constantin and Beyer 2016; Hoult et al. 2020); (iii) the second T-shaped unit tested by Brueggen et al. (Brueggen 2009; Brueggen et al. 2017), NTW2, which featured lap splices; (iv) other planar non-rectangular units with, e.g., barbell sections – apart from the abovementioned Units 1.0 and 2.0 (Mestyanek 1986), or essentially rectangular cross-sections with small flanges (Almeida et al. 2017); (v) lightly reinforced walls, which are not allowed in seismic regions as they form a single wide crack where yielding of reinforcement concentrates, instead of developing ductile response in the plastic region. The extension of the database for other non-planar walls is also possible, for example to include T-shaped walls with high-strength steel rebars (Burgos et al. 2024).

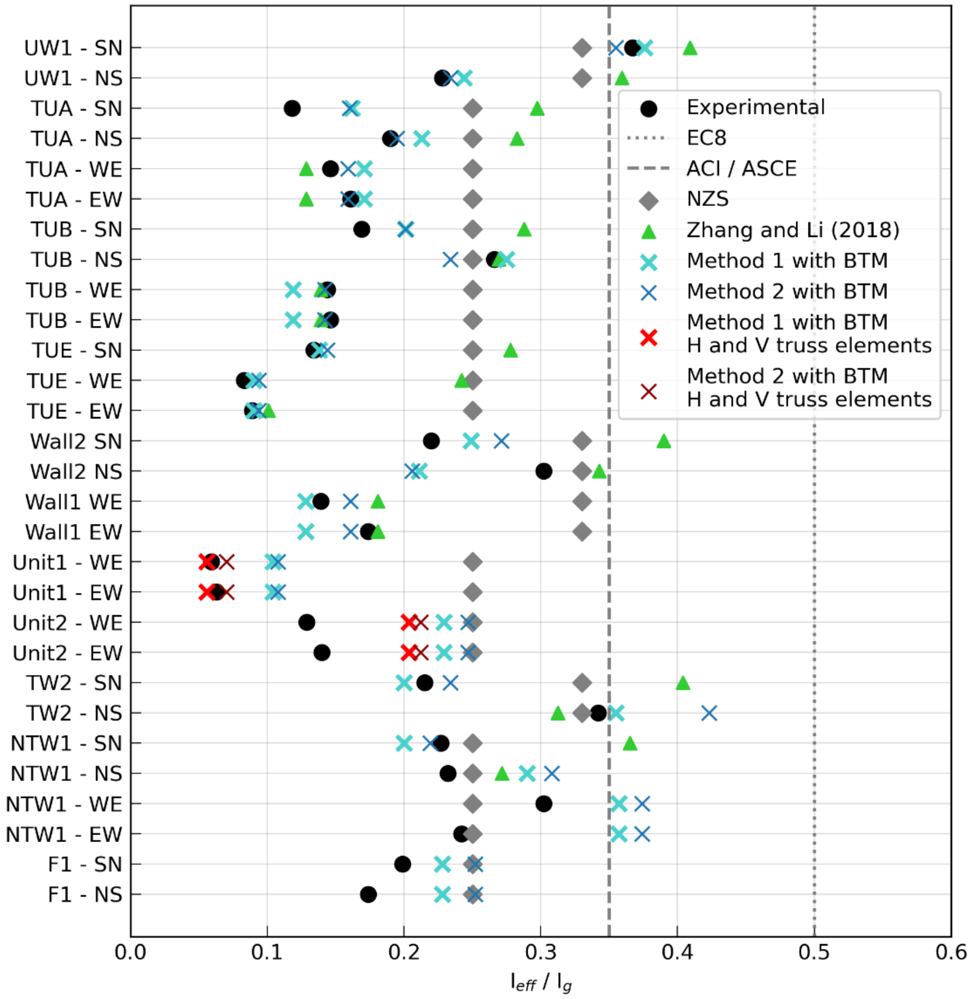

Figure 2. Comparison of the effective-to-gross moment of inertia ratios for the considered wall database, as computed from experimental data, beam-truss models, design code expressions, and literature.

Figure 2 plots, with black circular markers, the ratios of the effective-to-gross moment of inertia for the wall database identified above (excluding Wall3), as obtained experimentally, for which it is recalled the validity of the hypothesis $I_{eff} / I_g = K_{eff} / K_g$. The ratios are expressed in relation to the gross moment of inertia of each wall along the same direction. The difficulty in determining experimentally the occurrence of the first tensile yielding of the longitudinal reinforcement implied the adoption of Method 1, where V_{max} is the maximum experimental shear force along the direction under analysis. Method 2 will also be applied to the BTM results in Section 5.1. The dotted and dashed lines and the diamond markers in Figure 2 represent the values of effective stiffness ratios recommended by the design codes, whereas the triangular markers represent those proposed by (Zhang and Li 2018), according to the expressions summarised in Section 2.1. The latter do not include proposals for I-shaped wall sections (wall F1) nor along the minor axis of T-shaped wall (unit NTW1-WE and NTW1-EW).

Some initial conclusions can be drawn: (i) the experimental effective stiffness ratio for the set of walls varies roughly between 6% and 37.5%, with an average of 18.6% and a standard deviation of 7.9%; (ii) the effective stiffness of non-planar walls differs significantly among different cross-sections, loading axis, and direction of application of the load for asymmetric push/pull directions; (iii) code expressions significantly overestimate the effective stiffness ratios, and do so with disparate ratios; the (New Zealand Standard (2006) provides the best enveloping match to the experimental results, underestimating the effective stiffness just in a few cases; (iv) even with *ad hoc* formulas for the specific geometry, axis, and loading directions (Zhang and Li 2018), the effective stiffness of non-planar walls is difficult to estimate. Further comments will be provided in Section 5.1.

3 Beam-Truss Modelling and Application Examples

3.1 State-of-the-art review

The large number of factors influencing the effective stiffness of non-planar RC walls, combined with the observation that RC walls can assume a wide diversity of cross-sectional shapes, call for the application of numerical methods that, on the one hand, can be connected with practical use in FB design, and, on the other hand, are simultaneously applicable in the context of DB design and assessment procedures. In past (Kolozvari et al. 2018) and ongoing investigations, such as the project ERIES-ALL4wALL (Almeida et al. 2024) some of the state-of-the-art simulation techniques for RC walls are compared. The latter range from processor-heavy numerical approaches, including detailed FE simulations (Hoult and Almeida 2024) or the Applied Element model (Orgnoni and Pinho 2024), to other less computationally intensive methods, such as the multiple-vertical-line-element method (MVLEM). The latter extends the proposal by Vulcano et al. (1988), which itself refined the three-vertical-line-element model originally proposed by Kabeyasawa et al. (1983); today, it is mainly used in the so-called force-displacement version MVLEM-FD without (Fischinger et al. 2004; Janevski and Isaković 2024) and with shear-flexure interaction (Isaković and Fischinger 2019), or in another shear-flexure interaction approach with stress-strain relationships, denoted E-SFI-MVLEM-3D in its last version (Kolozvari et al. 2023). Other powerful and accurate models are undergoing continuous development (Suquillo et al. 2026; Tura et al. 2026). It is noted that, in the work by Kolozvari et al. (2018), the effective stiffness was computed for distinct modelling approaches, but it focused on rectangular walls.

The present investigation is intentionally restricted to the FEs most familiar to engineers, i.e. beams and trusses, since they appeal to a rather intuitive understanding of the involved structural mechanics. The most widely used beam theory, Euler-Bernoulli, is herein considered, to avoid the need of multi-axial material models and the increased complexity associated to higher-order deformation modes (Correia et al. 2015). Well-known constitutive models, associated to equally engineer-friendly cross-sectional fibre discretisations, are also adopted. Beams and trusses can be essentially found in all structural analysis software, from more research-oriented (McKenna 2011; SeismoSoft 2023) to more practice-oriented (Computers and Structures Inc. 2018) and, to the authors' knowledge, are widely used in practice to model RC walls. The simplest use of these models considers individual beam-column elements as a proxy for the entire wall, wherein the FE cross-section corresponds to the cross-section of the wall (Almeida et al. 2016); they are also known as line models and are commonly applied to slender members. A more detailed modelling of the wall cross-sectional segments (e.g. web and flanges in U-shaped wall cross-sections) via vertical elements, connected by horizontal links, has given rise to the so-called wide-column models (Beyer et al. 2008a); the definition of some input parameters for the latter approach is not exempt from contentious empirical considerations. The next level of modelling refinement with these FEs is the so-called Beam-Truss Models (BTMs); they will be adopted in the present study and are discussed in more detail further below. It is observed that neither BTMs nor wide-column models are discussed in a comprehensive review document (NIST 2017), although they are believed to be used in practice. To the authors' knowledge, the more refined application of truss elements to simulate reinforced concrete walls can be found in lattice modelling or bond-based peridynamics, which can be suitable to determine crack patterns, spacing, and other local engineering demand parameters (Aydin et al. 2019).

Nonlinear BTMs can essentially be regarded as a form of coarser three-dimensional lattice models, see Figure 3, which were originally used for the simulation of the experimental torsional and biaxial cyclic response of RC structural members (Miki and Niwa 2004). In short, vertical and horizontal elements represent concrete and reinforcement in those directions, whereas diagonal elements simulate the diagonal field of concrete in compression. This modelling strategy continued to evolve over the last two decades and is today a well-established and validated approach. Lu and Panagiotou (2012, 2014) contributed to its development through explicit consideration of the effect of normal tensile strain on the compressive behaviour of concrete in the diagonal direction – a feature that has been included in many BTMs since then, and mesh-size effects. In a subsequent study (Lu et al. 2016), the authors discussed the modelling of concrete tension in the horizontal direction and, among other modifications discussed below, suggested the following equation to determine the angle of the diagonal elements with respect to the horizontal:

$$\theta_{\mathrm{d}} = tan^{-1}\left(\frac{V_{max}}{f_{y,t}\rho_t t_w d}\right) \leq 65° \quad (1)$$

where V_{max} represents the maximum lateral force, the parameter ρ_t corresponds to the ratio of transverse reinforcement, with yield strength $f_{y,t}$, t_w is the thickness of the wall, and d is the distance between the outer vertical elements in the loading direction.

It is also recommended to have an angle θ_{d} greater than 45º, since an overly small angle can lead to grossly underestimating the maximum lateral force. If equation (1) yields $\theta_{\mathrm{d}} \geq tan^{-1}(H/d)$, where H is the height of the wall, the diagonal angle is governed by the wall geometry and the inclination is defined such that a continuous diagonal strut extends from the top corner to the opposite bottom corner of the wall. The BTM appears to best fit experimental results by having a similar angle for every diagonal element, large enough and close to the value obtained by equation (1).

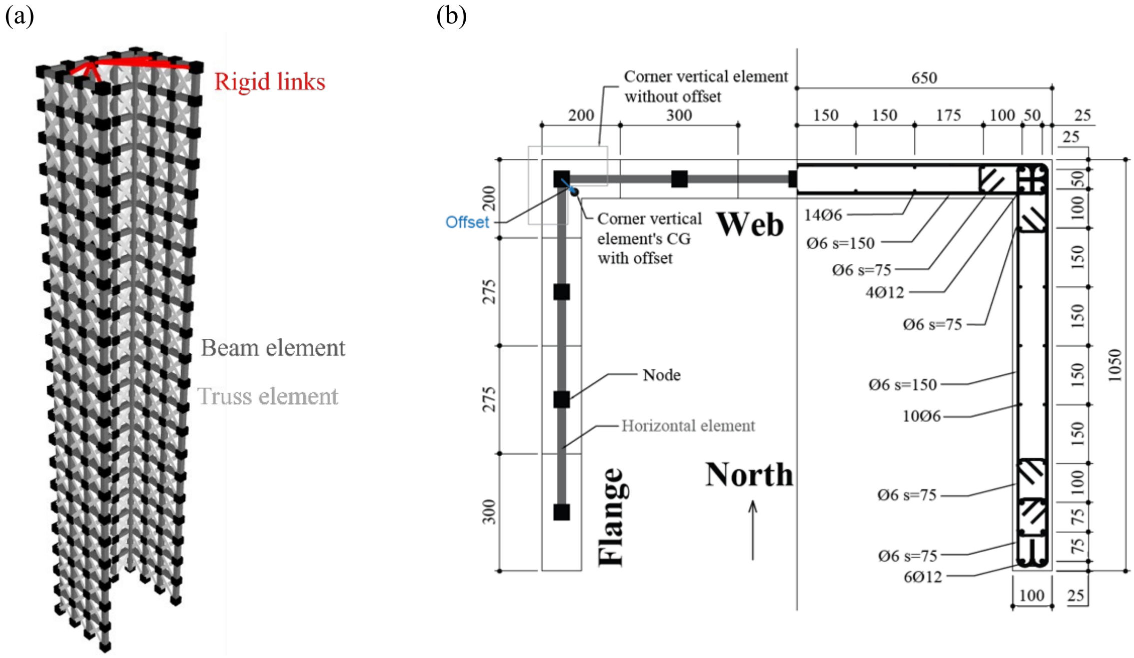

Figure 3. Illustration of BTM approach for the U-shaped wall UW1: (a) View of the global model, with rigid links connecting the top nodes; (b) Cross-section detailing and corresponding model discretisation, with corner element offset [dimensions in mm].

The extension of the BTM has continued over the last decade to incorporate additional deformation from failure mechanisms and loadings. Among others, the following contributions should be cited: (i) incorporation of rebar buckling and failure due to cyclic inelastic loading (Deng et al. 2021; Girgin et al. 2016); (ii) simulation of out-of-plane buckling (Álvarez et al. 2020); (iii) modelling of strain penetration in the foundation (Álvarez et al. 2020; Mavros et al. 2026); (iv) inclusion of lap-splice deformation and failure (Murcia-Delso et al. 2024) incorporating available expressions for the strain capacity of lap splices (Tarquini et al. 2019); (v) torsional response (Hoult et al. 2023b; Mavros et al. 2026).

Despite the recent developments and extensive applications described above, a generalized agreement on the modelling assumptions has not necessarily been reached. Namely, different authors have used different types of FEs (beams and trusses) and FE formulations, namely force-based and displacement-based (Almeida et al. 2016), to model the vertical and horizontal elements, as well as distinct connectivity releases at the nodes. Lu and Panagiotou (2012) used nonlinear fiber-section beam elements in the vertical and horizontal directions, and nonlinear trusses in the diagonal directions. In a subsequent work (Lu and Panagiotou 2014), the same authors replaced nonlinear by linear beams to simulate the horizontal elements. Later, the same team of researchers (Lu et al. 2016) made the point that, with the previous set of hypotheses, the BTM could not accurately capture diagonal tension failures because, by using beams with in-plane flexural stiffness for all vertical elements – which therefore resisted in-plane shear forces, the BTM did not allow the formation of in-plane mechanisms that represented diagonal tension failures. Hence, the previous authors proposed to pin, in the plane of the wall segment, the vertical elements that are not at the ends of the wall segment or at their intersection. Using nonlinear beams for the vertical elements that represent wall intersections, or the confined regions of planar walls, is generally considered an effective strategy to capture out-of-plane resistance and the vertical strain gradient in these regions. In the literature, it is still possible to find the use of beams for all vertical elements (Álvarez et al. 2020; Carrillo et al. 2022; Hoult et al. 2023a), whereas other research studies (Alvarez et al. 2019; Deng et al. 2021) are based on truss models for rectangular walls, i.e. nonlinear trusses are employed for all the elements including vertical ones. A range of beam FE formulations can be found in the literature: while some studies used force-based formulations (Lu et al. 2016; Lu and Panagiotou 2014), others have employed displacement-based approaches (Álvarez et al. 2020; Hoult et al. 2023b), as mentioned above. Displacement-based beam-column vertical elements have also been used to model the confined parts of walls in the simulation of coupled structural walls (Alvarez et al. 2019), or within an alternative modelling strategy that employs multi-layer shell elements in the unconfined wall regions (Mohammed and Barbosa 2019). Within the context of BTMs, considerations on the influence of the number of integration points when force-based elements are employed do not appear to have been investigated.

The effect of mesh refinement on BTMs has been studied by different authors. (Lu et al. (2014), for example, found a negligible effect on the force-displacement response, reporting a difference of less than 1% in the maximum roof drift ratio, during dynamic response, between a reference model and one in which the element size had been halved. Similar responses and failure modes were reported, but the authors also acknowledged the impact of mesh refinement on the magnitude of the computed strains. Álvarez et al. (2020) analysed the response of BTMs using two models, one with a fine grid and one with a coarse grid. They reported that, in general, mesh refinement did not affect the force-displacement responses. Other authors (Lu and Panagiotou 2012) observe that, when material softening was involved, mesh size effects were relevant for the computation of the force-displacement and strain responses. The above review highlights well-known issues of localisation in frame analysis (Almeida et al. 2016; Calabrese et al. 2010), and regularisation within the scope of BTMs (Lu and Panagiotou 2014). Regularisation techniques have been shown to provide highly similar results for walls with different mesh sizes (Deng et al. 2021).

Recently, BTMs have been successfully employed for larger scale simulations, from the cyclic response of seven-storey coupled structural walls (Alvarez et al. 2019) to nonlinear dynamic analyses of a 14-storey core wall building (Mavros et al. 2022, 2023), a high-rise 36-storey coupled-core wall building (Godinez et al. 2024), or the 15-storey Alto Rio building collapsed during the 2010 Maule earthquake (Zhang et al. 2017).

One relevant attribute of BTMs, in the scope of the current research on effective stiffness of walls with non-planar cross sections, compared with many other macroscopic models, is that BTMs do not impose a plane-section hypothesis, and account for axial-flexural-shear interaction.

3.2 *Simulation approach and limitations in engineering practice*

Despite the continuous development of BTMs described in the previous section, they also have limitations related to the underlying model hypotheses (Kolozvari et al. 2018). In particular, the overlapping areas of vertical, horizontal, and diagonal elements can compromise the accuracy of stiffness and strength simulations over the full range of displacement demand, from pre-cracking to collapse. To address this issue, some authors have scaled the stresses in vertical and inclined elements to account for the overestimation of the boundary region compressive resistance (Murcia-Delso et al. 2024). Moreover, the model may be sensitive to the chosen orientation of its composing elements – namely the diagonals, for loadings inducing significant variation of the principal compression stresses, e.g. as caused in coupled walls due to changing axial loading during seismic response.

Other challenges related to the application of BTMs are primarily practical. One concern is the computational demand required by too many degrees of freedom; however, BTMs have been successfully employed in complex nonlinear dynamic simulations of high-rise buildings (Godinez et al. 2024; Mavros et al. 2022, 2023; Zhang et al. 2017), demonstrating their engineering efficiency. Other difficulties arise with reference to the application of the angle given by equation (1). Firstly, since the bending capacity of non-planar walls along each loading axis and direction can vary, the walls also have different lateral force capacities, providing distinct values for the recommended diagonal angle θ_{d}. Additionally, there is a practical need to assign vertical mesh elements in the wall boundary regions with a cross-sectional length matching that of the respective boundary element, since these regions are usually assumed to have identical confinement. The previous requirement, together with the restrictions imposed by the finite length of each wall segment, as well as the specimen height (or inter-storey height, for a real building), typically constrain the adopted diagonal angle θ_{d}.

A pragmatic engineering compromise is therefore required. The wall BTMs developed in the current study favoured the adoption of a simple and systematic numerical simulation approach to all wall units, readily reproducible by practicing engineers. The software *SeismoStruct* (SeismoSoft 2023) was employed; a summary of the chosen modelling options is now presented. Following the discussion above and recommendations made in the previous sub-section, an extensive study was performed with several combinations of finite element types (beams and trusses) and formulations (force-based and displacement-based) for the vertical, horizontal, and diagonal elements, as well as different modelling proposals for the in-plane and out-of-plane connectivity of the intersecting nodes. Due to space limitations, the comparative results of all the models are not included. In brief, it was observed that the complexity of several of the explored options did not generally reflect on a net overall quality improvement in terms of global numerical-experimental match, instead it tended to trigger numerical convergence problems during the model response. Therefore, taking into account the convenience of application in engineering practice, particularly in terms of simplicity of model creation and numerical stability of the analysis, the modelling approach that was adopted is characterised by the following: (i) all horizontal and vertical elements of the BTM are modelled using nonlinear displacement-based FE beams (element "infrmDB" in *SeismoStruct*, with 2 Gauss-Legendre integration points), whereas diagonals are simulated by nonlinear truss elements; (ii) no specific allowances are made for releases of node connectivity between beam elements, either in-plane or out-of-plane; (iii) the angle suggested by equation (1) is followed to the extent possible, i.e. taking into account the limitations discussed above, where V_{max} was obtained from the experimental force-displacement curve along each loading direction; (iv) for each specimen, the mesh was defined to meet the constraints imposed by the wall geometry and reinforcement detailing of each cross-section, as previously noted. Figure 4 shows the mesh adopted for each wall model, with element sizes comparable to those used by other authors modelling similar units. Simple parametric studies with alternative refinement levels were conducted to ensure objective global (force-displacement) and local (strain demand) responses during the phase relevant to the determination of effective stiffness. As discussed in the previous sub-section, localisation effects and regularisation techniques may become relevant in the softening range but are of limited importance for the present study. Nonlinear geometric effects were included.

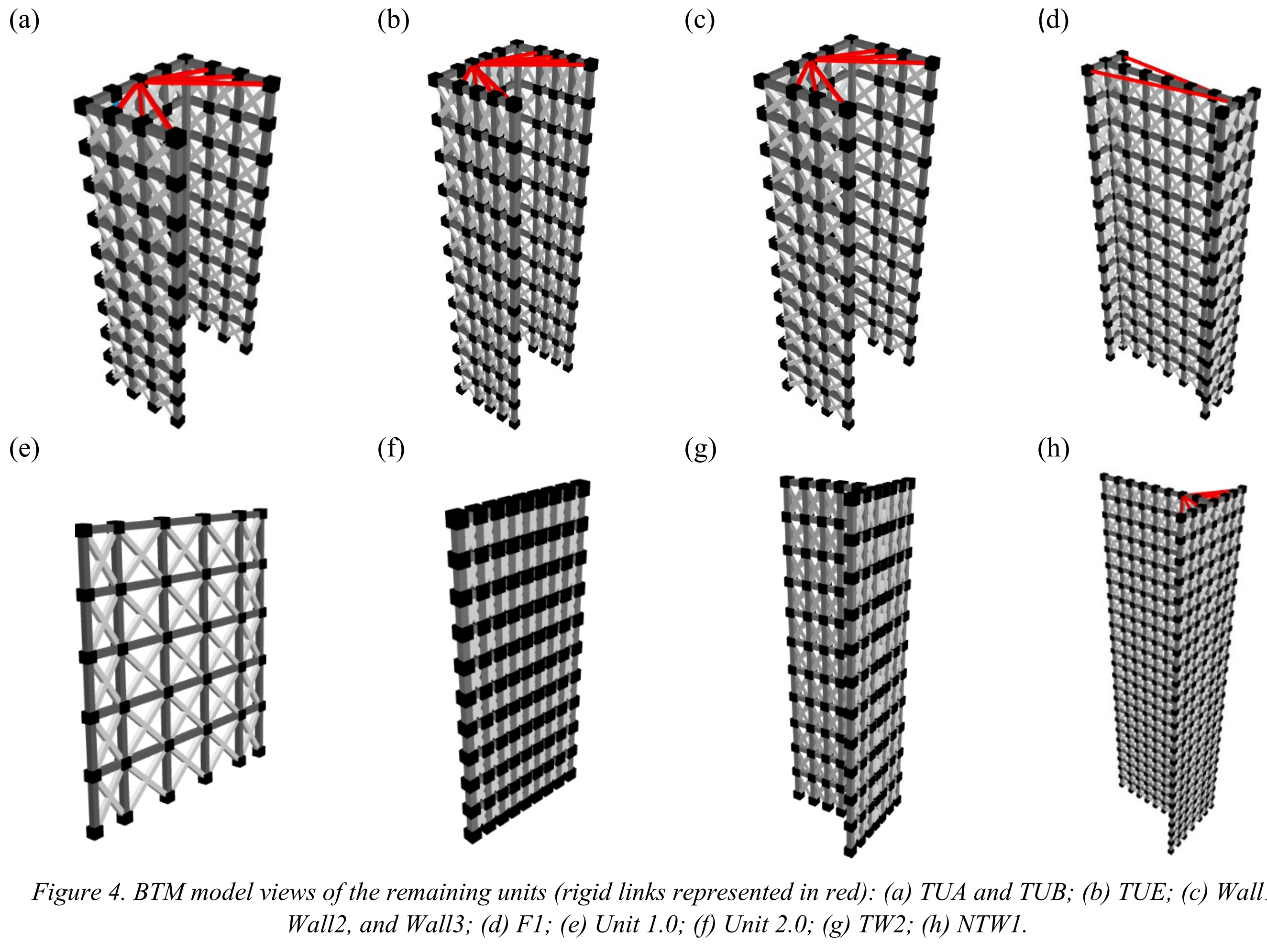

Figure 4. BTM model views of the remaining units (rigid links represented in red): (a) TUA and TUB; (b) TUE; (c) Wall1, Wall2, and Wall3; (d) F1; (e) Unit 1.0; (f) Unit 2.0; (g) TW2; (h) NTW1.

Some of the wall BTM vertical elements, namely in the boundary regions, contain longitudinal reinforcement and additional hoops in confined regions. Other vertical FEs do not require the assignment of transverse reinforcement as it is considered that confinement is negligible; this is also the case of the horizontal elements, whose longitudinal reinforcement is composed of the transverse rebars in the specific wall segment. For these horizontal elements and vertical elements outside the confined boundary-element regions, the transverse steel reinforcement was set to a numerical zero (i.e. negligible reinforcement ratio), which results in an automatically computed confinement factor of 1. Truss elements for the diagonals have full concrete sections without reinforcement.

The material properties can be summarised as follows: (i) reinforcing bars are simulated with the Menegotto-Pinto model (Menegotto and Pinto 1973); the fracture strain parameter is adjusted to 60% of the fracture strain reported from the available experimental monotonic tests, to account for buckling and low-cycle fatigue; (ii) concrete is simulated with the nonlinear model proposed by Mander et al. (1988), assigning the compressive strength reported from available tests as the mean strength; wherever experimental tensile strength results are not available, its value was determined according to Eurocode 2 (CEN 2004b). As adopted by others, the tensile strength of the concrete in the diagonal elements was ignored (Arteta et al. 2019; Lu et al. 2016) and no reinforcement is considered in its cross-section, as mentioned above. The tensile strength in the horizontal elements was also ignored (Álvarez et al. 2020; Lu et al. 2014, 2016). It is noted that the numerical tests accounting for the tensile strength either in the horizontal or diagonal elements tended to create numerical instability, manifested in the form of short peaks and troughs in the pushover response. In summary, tensile strength is only assigned to the vertical elements.

The wall models were subjected to a constant axial load and a history of static lateral displacements according to the respective experimental program, or to pushover. The reinforced concrete self-weight is assigned to the density of the reinforcement and the concrete of the BTM vertical elements, whereas the horizontal beams and diagonal trusses are considered weightless.

During the analyses, various control points are defined to represent the following limit states in the vertical elements, related with the outermost cover and confined concrete fibre strains (compressive strains are defined as negative), and outermost steel rebar strains: (i) concrete crushing, $\varepsilon_{c,crushing} = -0.002$; (ii) steel rebar yield strain, ε_y, corresponding to the yield strain reported experimentally; (iii) steel rebar fracture strain, ε_{su}, which as discussed above was assigned a value corresponding to 60% of the fracture strain reported experimentally; (iv) ultimate compression strain for confined concrete, $\varepsilon_{cu,c} = -0.004 - \frac{1.4\rho_s f_{ym}\varepsilon_{su}}{f_{cm,c}}$, where ε_{su} refers to the confining reinforcement fracture strain, f_{ym} represents the confining rebar yield strength, ρ_s is calculated as the proportion of steel volume in the BTM vertical element representing the wall boundary element, and $f_{cm,c}$ is the confined compressive concrete strength (Priestley et al. 2007).

Whereas the first two limit states are directly linked with Method 2 for the computation of the effective stiffness (refer to Section 2.1), the last two relate to the calculation of V_{max}, and consequently to Method 1. Such limit states leave out several other damage modes, including lap-splice slip, shear sliding, inclined (shear) cracks, etc. Rebar buckling and low-cycle fatigue are indirectly accounted for, in a simplified way, by the application of the aforementioned factor of 60% to the steel rebar fracture strain. For a more extensive consideration of damage states associated with different performance levels, one can refer, for instance, to the recent work by (Murcia-Delso et al. 2024).

Since the BTM wall models strictly followed the above-described procedure and were not optimised on a unit-by-unit basis for improved match with the experimental response, nor included some of the most recent model refinements as reported in the previous sub-section, the results are anticipated to be subpar with respect to the more advanced versions of the BTM. For most code-designed walls with shear span ratios not too small, i.e. excluding squat and intermediate walls with SSRs up to approximately 2, more advanced modelling is not expected to significantly change effective stiffness estimates or the simulation of nonlinear response up to steel yielding and during the earlier phases of inelastic behaviour. However, it can affect the simulation accuracy related to the onset of strength degradation, and thus wall displacement capacity, when: (i) diagonal concrete softening and crushing takes place; it is noted that the FE formulations implemented in *SeismoStruct* do not yet directly allow to account for the effect of the diagonal normal tensile strain on the compression strength; (ii) an accurate modelling of rebar buckling is desirable; (iii) global out-of-plane buckling of a wall segment end is relevant; (iv) rebar strain penetration in the foundation significantly contributes to the wall deformation, or anchorage failure occurs; (v) torsional demands are large; (vi) particular construction details are present, such as lap splices.

3.3 Application example I: Uniaxial loading

This section details the BTM modelling approach to wall unit UW1, as an example of the simulation approach described before and applied to all wall units in Section 4.1. The specimen, whose geometry and detailing of the U-shaped cross-section are depicted in Figure 1 (a), was tested by Hoult et al. (2023c) in the Institute of Mechanics, Materials and Civil Engineering (iMMC) at Université catholique de Louvain (UCLouvain), Belgium.

The BTM of UW1, shown in Figure 3 (a), has a total height of 6720 mm, corresponding to the shear span effectively applied during the test. The lateral displacement results presented in Figure 5 refer, however, to a height of 2250 mm, which is the height of the wall collar at which the actuators were connected. An axial load ratio (ALR) of 5% was also applied to the test unit and the model. The nodes at the base are assigned full fixity. The wall top nodes are connected through rigid links to a master node, as illustrated in Figure 3 (a), to which the incremental displacement is imposed; the slave nodes are restrained only along the two horizontal directions, i.e. the rotation along the three axes, as well as vertical displacements, are not restrained. Figure 3 (b) shows the discretisation of the BTM vertical elements in the cross-section, whereas Figure 3 (a) shows the discretisation along the wall height. This discretisation resulted from the following constraints, some of which were discussed in Section 3.2: (i) length of the confined boundary element regions (i.e. flange ends and flange/web intersections); (ii) the angle suggested by equation (1), which herein provides a value of $\theta_d = 47.3°$; (iii) the need to monitor the lateral displacements at a height of approximately 2250 mm, for comparison with experimental results. Figure 3 (b) also illustrates a more specific detail, namely the application of a diagonal offset to the corner vertical elements in the intersection between the web and the flange, to account for the fact that aligning the corresponding centre of gravity (CG) with the CG of the neighbouring elements along the web and along the flange would result in an incorrect positioning of such corner elements. A similar BTM model for the same unit was employed by Hoult et al. (2023b). An acceptable comparison between experimental and numerical results is shown in Figure 5, together with the discussed limit state strains. The slight difference in simulated strength towards the south is likely to be due to the fact that, experimentally, the application of the axial load caused a small overturning moment that is not accounted for numerically. The pushover analyses along the south-north and north-south directions, depicted in Figure 7 (a) and used to compute the effective stiffness, correspond approximately to the envelope of the cyclic response.

3.4 Application example II: Biaxial loading

The ability of BTMs to simulate the cyclic response of units subjected to biaxial lateral loading is illustrated herein with three walls. The details of the three U-shaped wall units can be found in the corresponding publication by (Ile and Reynouard (2005). The walls share the same dimensions, material properties, and reinforcement details; the cross-section can be seen in Figure 1 (b).

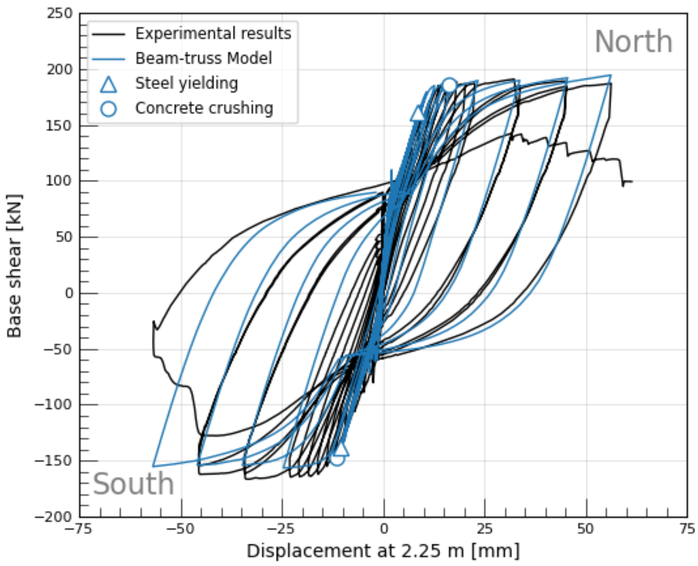

Figure 5. Experimental cyclic results of unit UW1 and comparison with BTM, with indication of limit state strains.

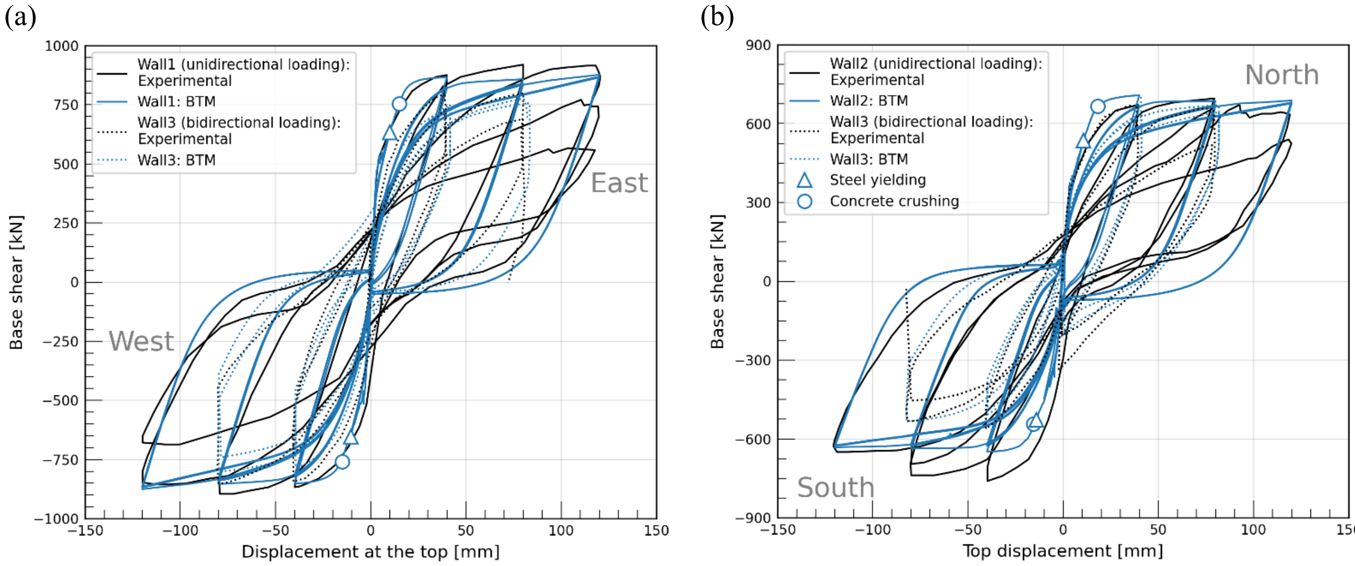

Figure 6. Experimental test results of Wall1, Wall2, and Wall3 by (Ile and Reynouard (2005), and comparison with BTM results, along: (a) west-east direction; (b) south-north direction.

The units were loaded differently: while Wall1 was tested along the major (west-east) axis and Wall2 along the minor (south-north) axis, Wall3 was subjected to a biaxial "butterfly" loading protocol (Ile and Reynouard 2005). Therefore, this latter unit included loading phases both along the major and minor axes, which can be compared in Figure 6 with the individual response along each loading axis of Wall1 and Wall2 (black solid versus black dotted lines). The same figure includes also the simulation output given by the BTM – in solid and dotted blue lines, showing a good agreement with the test results. A critical interpretation of these results will be made later, in Section 5.4, to comment on the associated effective stiffness.

4 Comparison of Numerical and Experimental Results

4.1 Complete database summary

Figure 7 shows the BTM pushover results obtained along the two main perpendicular directions (major and minor axes) of the selected database of wall units indicated in Section 2.2, together with the experimental cyclic response. The computational time for the pushover analysis of each wall was typically less than 1 minute in a laptop with an Intel Core i7-1355U CPU, 16 GB RAM, running Windows 11 (64-bit). Although an in-depth analysis of the results is beyond the scope of this study, a critical comparative overlook shows that, despite some discrepancies, the BTM provides a good agreement with the envelope of the units' cyclic responses, particularly until the attainment of first yield or concrete crushing. These values are used to compute the effective stiffness according to Method 2. It is also noted that, for most of the simulations, the first yield of longitudinal reinforcement was attained at a drift smaller than that corresponding to the cover concrete crushing. In this respect, and as expected, the least accurate match in terms of stiffness at first yield or concrete crushing occurs for Unit 1.0 and Unit 2.0, where there is a relatively early departure from the experimental measurements. These cases are analysed in more detail in the next sub-section.

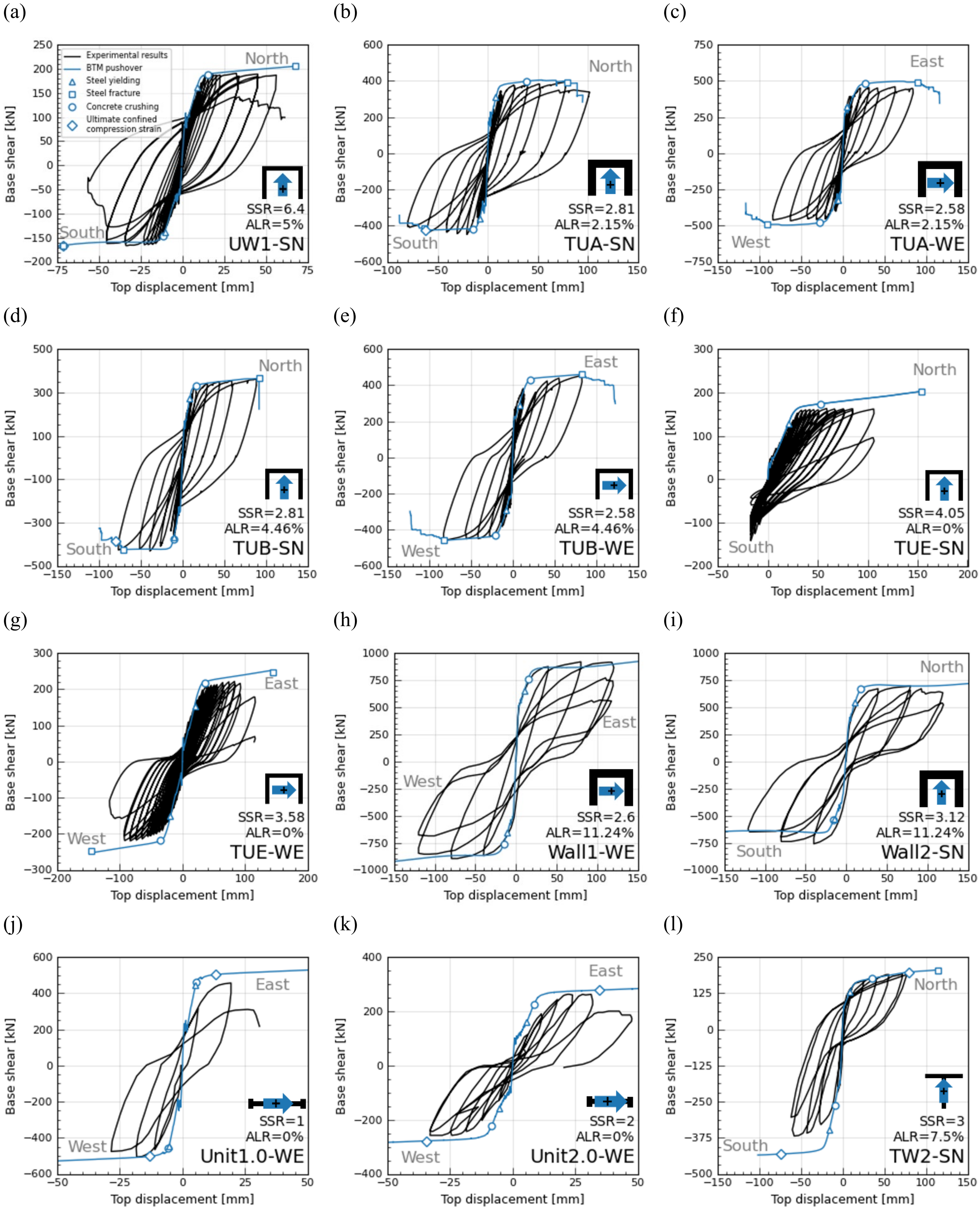
(a)
Experimental results
BTM pushover
Steel yielding
Steel fracture
Concrete crushing
Ultimate confined compression strain
North
South
SSR=6.4
ALR=5%
UW1-SN
(b)
North
South
SSR=2.81
ALR=2.15%
TUA-SN
(c)
East
West
SSR=2.58
ALR=2.15%
TUA-WE
(d)
North
South
SSR=2.81
ALR=4.46%
TUB-SN
(e)
East
West
SSR=2.58
ALR=4.46%
TUB-WE
(f)
North
South
SSR=4.05
ALR=0%
TUE-SN
(g)
East
West
SSR=3.58
ALR=0%
TUE-WE
(h)
East
West
SSR=2.6
ALR=11.24%
Wall1-WE
(i)
North
South
SSR=3.12
ALR=11.24%
Wall2-SN
(j)
East
West
SSR=1
ALR=0%
Unit1.0-WE
(k)
East
West
SSR=2
ALR=0%
Unit2.0-WE
(l)
North
South
SSR=3
ALR=7.5%
TW2-SN
Base shear [kN]
Top displacement [mm]

(m) (n) (o)

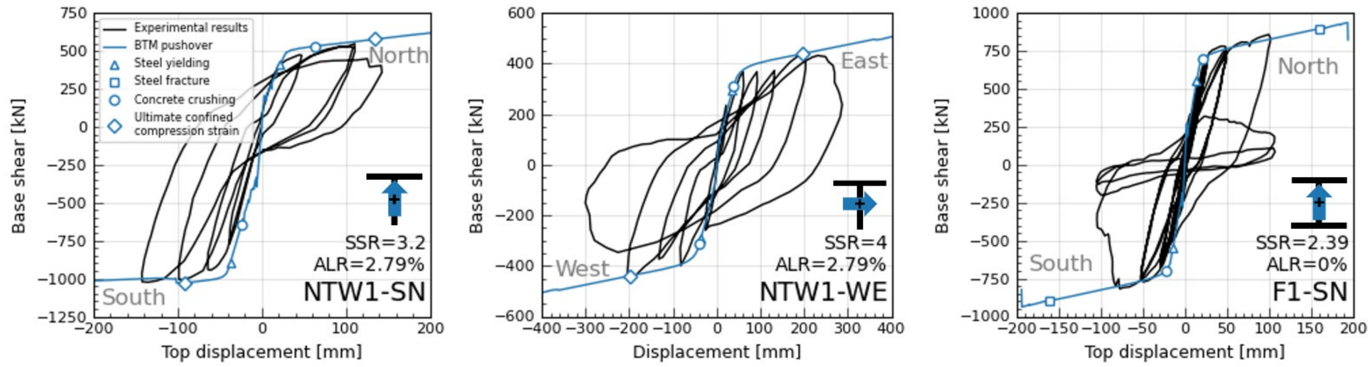

Figure 7. Pushover results for unit: (a) UW1, south-north; (b) TUA, south-north; (c) TUA, west-east; (d) TUB, south-north; (e) TUB, west-east; (f) TUE, south-north; (g) TUE, west-east; (h) Wall1, west-east; (i) Wall2, south-north; (j) Unit 1.0, west-east; (k) Unit 2.0, west-east; (l) TW2, south-north; (m) NTW1, south-north; (n) NTW1, west-east; (o) F1, south-north.

The prediction of the displacement capacity is more challenging, due to the reasons pointed out in Section 3.2 and the fact that the full cyclic response is not herein simulated. It should be emphasised that this study does not aim to accurately simulate displacement capacity, since it does not influence the computation of effective stiffness of slender walls incorporating basic seismic design considerations and hence some ductility. Nonetheless, for several units, the attainment of steel fracture or ultimate compression strain for confined concrete provides a reasonable estimate when compared to the experimental response. Regarding the specimens' force capacity V_{max} associated with the same two limit states, it can be observed that the numerical-experimental agreement is overall very satisfactory, as it will also be apparent in Section 5.1 through the application of Method 1 for the computation of effective stiffness. The exception is the north-south direction of unit TW2, which is also analysed in further detail in the next sub-section.

4.2 Remarks on some key modelling assumptions

The current sub-section briefly addresses the cases where the numerical-experimental mismatch is more pronounced. Namely, it considers Unit 1.0, Unit 2.0, and the north-south direction of TW2. It is noted that Unit 1.0 and Unit 2.0 correspond to squat and intermediate walls, respectively, and were included to examine the limits of the modelling approach at lower SSR values, as discussed in Section 2.2. These tested walls are seen to be less stiff than the numerical response, which is attributed to the experimental cracking, softening, and crushing along the diagonal, deficiently captured by the adopted version of the BTM, as discussed in Section 3.2. This deviation arises not only from neglecting the influence of biaxial strains on the concrete's compressive behaviour along the diagonals, as anticipated in Section 3.2, but also because the flexural stiffness of the internal vertical elements, i.e. not located at the wall ends, significantly increases the numerical stiffness of the wall (Lu et al. 2016). Therefore, Units 1.0 and 2.0 were alternatively modelled using truss FEs for all elements – including the vertical and horizontal ones, except the vertical boundary ends which were kept as DB beams. As shown in Figure 8, the latter approach reduced the force capacity of the specimens, bringing it closer to the experimental results. More importantly for the estimation of effective stiffness, the pushover analysis of the squat Unit 1.0 follows the envelope of the experimental cyclic response more closely, while the intermediate Unit 2.0 shows only a limited enhancement. The new effective stiffness ratios obtained using Methods 1 and 2 are much closer to the experimental values for Unit 1.0, as shown in Figure 2, whereas only limited improvement was observed for Unit 2.0 compared with the previous modelling approach, which will be discussed in Section 5.1.

Both Units 1.0 and 2.0, with barbell-shaped cross-sections, are classified as non-planar. However, the applied in-plane loading does not fully reveal the challenges typically associated with modelling walls composed of two or more perpendicular segments. In such cases, the structural response may become unrealistic because truss elements can develop local mechanisms of Type III or IV, as identified by Feron et al. (2024), in the loading-perpendicular direction, meaning that large portions of wall segments may not participate in the response. One way to address this is to assign distinct connectivity releases at the nodes according to the loading direction, allowing some elements to exhibit a mixed truss-beam behaviour. This approach, however, is cumbersome, lacks clear physical interpretation, and often leads to numerical difficulties. Additionally, for slender members, the numerically predicted deformations may also diverge from the actual response. The difficulty in reproducing the deformed shape is evident for wall TW2 under north–south loading when modelled using a truss-based strategy similar to that adopted for Units 1.0 and 2.0, but modified to include vertical elements in the web to prevent the aforementioned local mechanisms. In fact, although the force–displacement curve in Figure 8 (c) suggests significant improvement, the corresponding deformed shape (shown in the inset) differs markedly from the experimental observations (Thomsen IV and Wallace 1995), with shear deformations at mid-height greatly overestimated and flexural deformations at the base highly underestimated. The specific reasons for this discrepancy in the north–south response of wall TW2 warrant further investigation. It is worth noting, however, that Orakcal et al. (2006) and Lu and Panagiotou (2012) also reported similar difficulties, including strength and stiffness overestimations, when attempting to reproduce the experimental response of TW2 along this direction.

In summary, the modelling approach adopted in this study, described in Section 3.2, is easy to implement and appears to provide reliable results in terms of both accuracy and numerical stability for ductile, flexure-dominated walls, which are predominant in current medium- to high-rise building design. For other cases as noted at the end of Section 3.2, such as squat walls, specific model adaptations may be required.

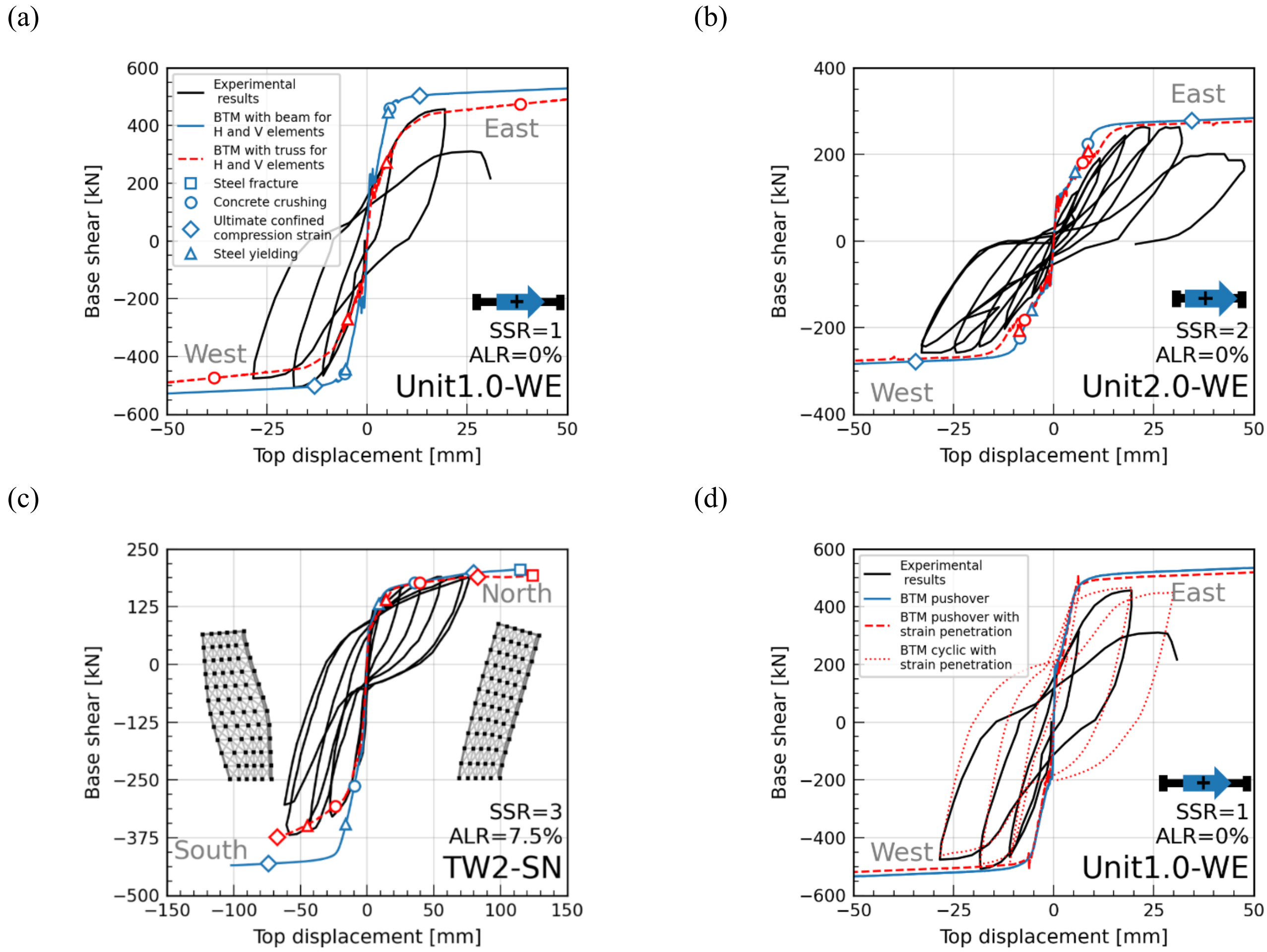

Figure 8. Effect of the choice of finite element types (beams or trusses) on the pushover results, for wall specimens: (a) Unit 1.0; (b) Unit 2.0; (c) TW2, including insets illustrating the deformed shape at a drift of 2.5%; (d) Effect of strain penetration and cyclic response for Unit 1.0.

A final consideration is made regarding another key modelling assumption. Among the factors listed at the end of Section 3.2, the one most likely to affect the response of intermediate or slender code-designed walls is strain penetration into the foundation. Tastani and Pantazopoulou (2015) showed that strain penetration occurs not only in the footing but also over a significant portion of the wall height, concluding analytically that yield penetration can increase compressive strains at the wall toes. More recently, several researchers have explicitly modelled strain-penetration effects in FE analyses of RC walls, with varying levels of refinement and assumptions (Dameh and Pantazopoulou 2024; Hoult and Almeida 2024; Tura et al. 2026), supported by comparisons with new experimental evidence from distributed fibre-optic sensors along longitudinal reinforcement (Hoult et al. 2023c). In the context of BTMs, the simulation of this phenomenon is still at an early stage, but initial efforts have been made. In particular, Álvarez et al. (2020) proposed an approach in which all degrees of freedom at the wall-foundation interface are fixed except the vertical one. The latter accounts for strain penetration deformation arising from auxiliary vertical truss elements representing reinforcement embedded in the foundation. More recently, Mavros et al. (2026) investigated strain penetration effects in BTMs using two alternative modelling approaches, alike to Álvarez et al. (2020), but differing in the node releases and constitutive relations;

application to wall unit UW1 showed that strain penetration delayed reinforcement failure and somewhat improved agreement with experiments, although the effect was not significant for this specific unit. In the current study, to gain a preliminary understanding of the potential influence of strain penetration, some units were also modelled following the approach proposed by Álvarez et al. (2020). The vertical truss elements embedded in the foundation were assigned the same cross-sectional properties as the wall vertical elements to which they are connected, with concrete modelled as elastic in compression and without tensile strength, steel models and parameters identical to those of the wall reinforcement, and element length taken as L_{sp} = 119 mm as defined by Priestley et al. (2007). The results, not shown here due to space limitations, indicate that strain penetration had only a minor effect on the global force-displacement responses, as well as on the effective stiffness, underscoring the need for further investigation of this topic in future studies. For illustration purposes, Figure 8 (d) shows the influence of strain penetration on the response of Unit 1.0, as well as its combined effect with cyclic loading.

5 Effective Stiffness and Axial Load

5.1 Assessment of the effective moment of inertia

The ratios effective-to-gross moment-of-inertia for the wall units, as simulated with BTMs in the previous section, are added in Figure 2 with cross markers, according to the two methods introduced in Section 2.1. For the application of Method 1 to the BTM results, V_{max} is determined based on the attainment of the steel rebar fracture strain ε_{su} or the ultimate compression strain for confined concrete $\varepsilon_{cu,c}$, along the direction under consideration, whichever occurs first.

One first observation is that, for most units, Method 1 and Method 2 provide rather similar estimates of the effective stiffness. Additionally, apart from some units and directions, the match between the effective stiffness ratios computed from the BTM models and the experimental tests is satisfactory, which points to its applicability in engineering practice.

To better highlight the accuracy of the different approaches, namely design code expressions, literature, BTM – Method 1, and BTM – Method 2, applied to the wall database, the results of Figure 2 are replotted in Figure 9 in the form of relative differences with respect to the effective stiffness obtained from experimental data. Table 2 shows the average relative difference and standard deviation for the 29 estimates of the effective stiffness. The variability and conservatism of the design code expressions is quite significant, reducing progressively from the current and next generation of Eurocode 8 (CEN 2004a, 2024), to the American codes ACI 318-9 (American Concrete Institute 2019) and ASCE/SEI 41-17 (American Society of Civil Engineers 2017), and finally to the New Zealand Standard (2006). A subset of the database, composed of the T-shaped units loaded along the major axis, as well as U-shaped walls, is compared in the last two columns of Table 2 with the expressions proposed in the literature by Zhang and Li (2018). The latter perform only slightly better, on average, than the expressions in the New Zealand code. Unsurprisingly, the best estimates are provided by the BTM – Method 1 and the BTM – Method 2, which output an average relative difference on the entire database of 15% and 21%, respectively, as well as the smallest variations among units.

Table 2. Comparison of the different approaches to estimate the effective stiffness of RC walls in the database.

Different approaches	Entire database (29 estimates of effective stiffness)		Only for U-shaped and major-axis-bending T-shaped walls (21 estimates of effective stiffness)	
	Average relative difference [%]	Standard deviation of the relative difference [%]	Average relative difference [%]	Standard deviation of the relative [%]
Eurocode 8	229	175	198	123
ACI 318-9 and ASCE/SEI 41-17	130	122	108	86
New Zealand Standard	74	84	62	58
Zhang and Li (2018)	/	/	48	60
BTM - Method 1	15	29	2	17
BTM - Method 2	21	30	6	16

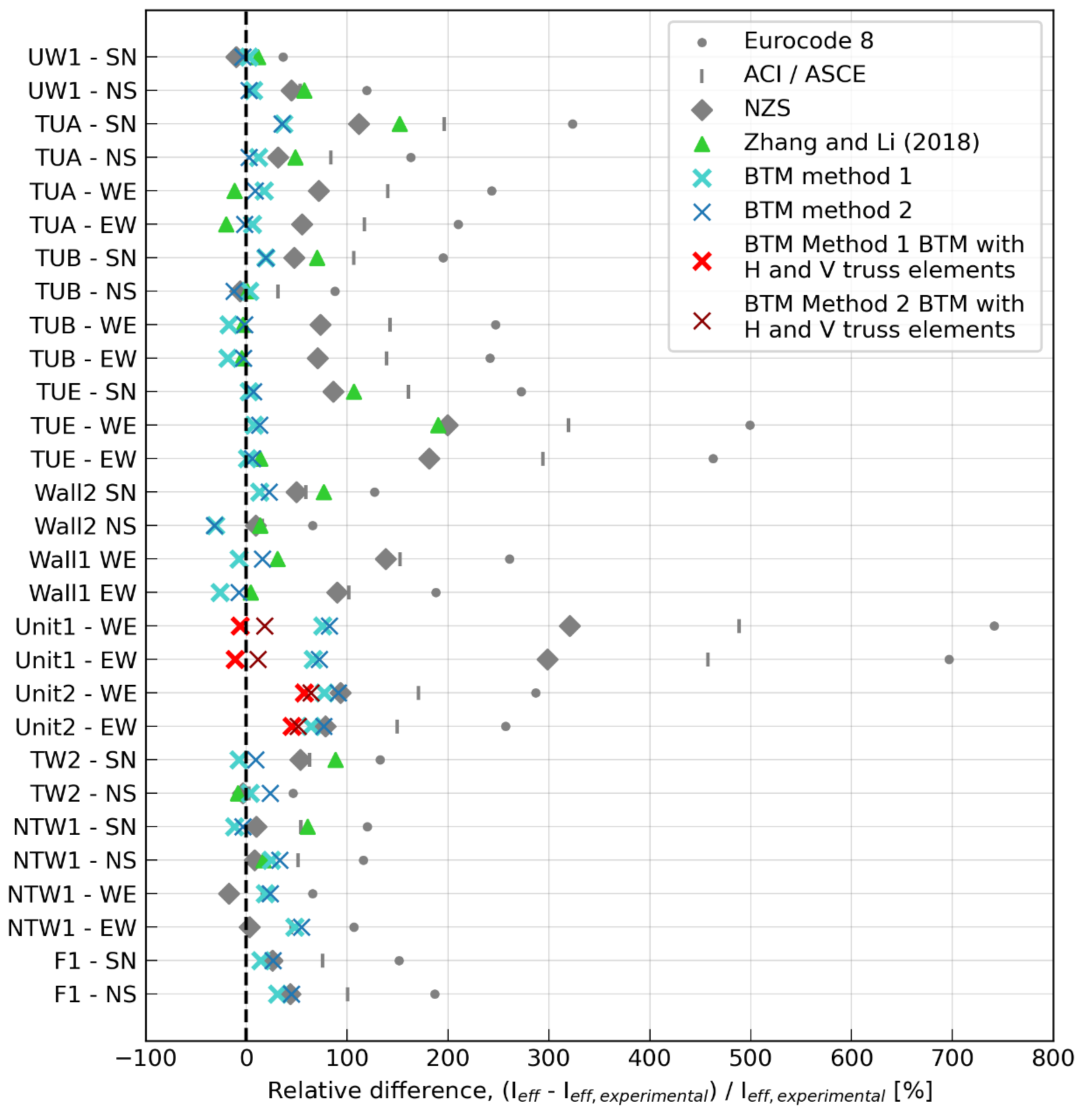

Figure 9. Relative difference of numerically estimated / codified / proposed effective stiffness with respect to that calculated from experimental test results, for the considered wall database.

The positive deviation of the average relative difference for the BTM's effective stiffness can be explained, to a large extent, by the four data points for which the BTM estimated a higher value, corresponding to the walls Unit 1.0 and Unit 2.0 by Mestyanek (1986). Upon first impression, the latter could be considered easier to simulate because of their planar cross-section (even though non-rectangular), but as explained previously the specific limitations of the herein-employed BTM prevented an accurate tracking of the experimental deformation and failure modes. Moreover, it is noted that several modelling assumptions in the BTMs employed in the current study were not optimised on a unit-by-unit basis, as discussed in Section 3.2. Had such optimisation been performed, the already small scatter in the BTM-experimental relative differences would likely have been even further reduced.

5.2 Influence of Axial Load Ratio

The review in Section 2.1 highlighted the applied ALR as one of the key factors known to affect the effective stiffness of RC walls. The present paragraph briefly addresses the influence of this parameter employing the described BTMs and compares the results with estimates provided in the specialised literature (Zhang and Li 2018). As case studies, two walls with different cross sections are analysed herein. In particular, the U-shaped wall unit TUB (Beyer et al. 2008b) is subjected to an ALR varying from 0 to 20%, while the T-shaped wall TW2 (Thomsen IV and Wallace 1995) is loaded with an ALR changing between 0 and 15%. The variation of the effective stiffnesses with the ALR, using BTMs, is shown in Figure 10 (a) and (b) for TUB and TW2 respectively, along different axes and directions. As a starting observation, Figure 10 (a) shows that, as discussed previously, both Methods 1 and 2 yield similar values, with noticeable deviations appearing at higher axial load ratios (ALR).

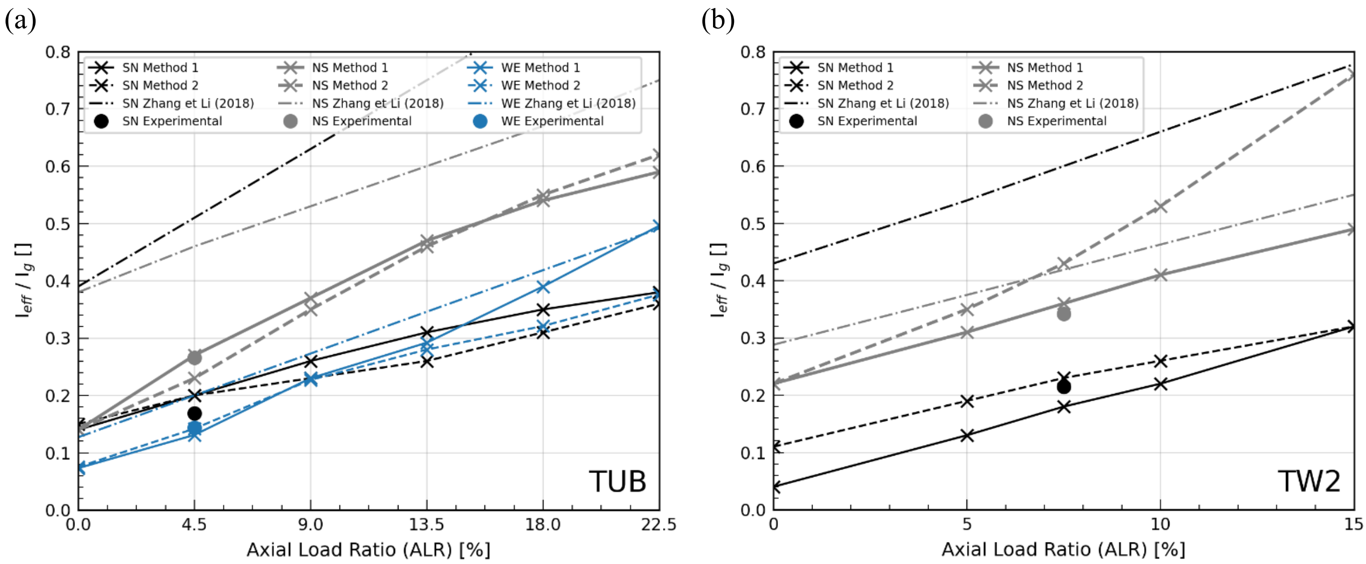

Figure 10. Influence of axial load ratio on effective stiffness, as predicted by BTMs and literature expressions, for: (a) wall TUB; (b) wall TW2.

The figure confirms that a positive variation of the ALR increases significantly the effective stiffness; for the relatively restricted ALR interval of 5-15%, common in real buildings, the effective stiffness of both TUB and TW2, about all axes and loading directions, roughly doubles. The effective stiffness appears to vary almost linearly with the ALR, although the corresponding slope changes substantially as a function of the loading axis and loading direction. The authors obtained a similar conclusion for other walls in the database, whose results are not shown. At the intercept, i.e. for ALR=0%, the effective stiffness of TUB as computed with BTMs for the south-north and north-south directions is approximately the same, whereas very different values can be found for TW2 at ALR=0%. Unsurprisingly, the slope and the intercept vary for the perpendicular cross-sectional loading axis (west-east, or similarly east-west) of TUB. Finally, it is observed that closed-form expressions from the literature fail to reproduce the numerically obtained results.

5.3 Influence of Axial Load Eccentricity

RC walls resist gravity-induced shear forces transferred from the connected horizontal structural members, and therefore the axial load resultant from gravity applied to most walls in RC buildings is never coincident with the corresponding cross-sectional centre of gravity. This axial load eccentricity can be small – for example for interior walls in buildings with regular symmetric spans, or more significant – namely for walls in the building periphery. Additionally, this eccentricity can occur along both axes simultaneously. An accurate estimation of the axial load applied to a specific wall, under gravity loading, as well as the corresponding eccentricity along both axes, typically requires setting up a finite element model of the building. Alternatively, a rougher approximation can be obtained by more straightforward computations of the mass in the surrounding influence area. As far as the authors are aware, the influence of the axial load eccentricity on the wall effective stiffness has not yet been addressed in the literature, and it is also not included in design or assessment expressions for wall effective stiffness. This section provides a first insight on the potential relevance of such variable.

The wall units UW1, TUB, and TW2 (see Figure 1) are again revisited as illustrative case studies. The ALR considered for the analyses correspond to the actual value of ALR applied in the corresponding experimental test, i.e. 5.0%, 4.5%, and 7.5% respectively. Figure 11 (a) shows, for these three units and employing Method 1 for the calculation of the effective stiffness, the influence of eccentricity. The latter is varied, with respect to the centre of gravity, within the relatively narrow range of ± 25% of the wall segment length in the direction of bending (i.e. the flange length in UW1 and TUB for bending about the minor axis, and the web length for TW2 and UW1 along the major axis). A positive eccentricity corresponds to an eccentricity in the direction of the applied loading. The first main comment to the plotted results is that even minor variations in the eccentricity, which are likely to occur in built structures, can substantially impact the effective stiffness; such influence is comparable to that of the ALR discussed in the previous sub-section. Although the slopes for most of the loading axes and directions are approximately identical, the variation for TW2 along the south-north direction indicates that it is dependent on the cross-sectional shape.

The value of the ALR applied experimentally to the considered units, in particular units UW1 and TUB, is likely to fall on the lower end of the wall ALR at the bottom storey of many real multi-storey buildings. This constraint is typically due to the insufficient force capacity of most laboratory actuators to impose higher and more representative values of axial loads. To study this aspect, Figure 11 (b) compares the response of UW1, loaded along the south-north direction, for a range of ALRs, namely 5% (i.e. the experimentally applied value), 10%, and 15%. The impact on the effective stiffness variation is unequivocal, with a sharp change in slope for different ALRs.

It can be observed that, for the higher positive eccentricities, the effective stiffness is less dependent on the ALR. In these cases, the bending moment caused by the axial load eccentricity pushes the neutral axis to the compressed web of the U-shaped wall, with minor variations in its position during pushover in the same direction. For negative eccentricities, the two flanges' extremities are initially compressed; during pushover, the cross section retains a larger proportion of its gross moment of inertia as the compressed region progressively moves towards the web. Figure 11 also plots the specific expressions in the literature (Zhang and Li 2018), which do not account for the eccentricity. The findings in this section underscore the importance of explicitly modelling core walls (e.g. with BTMs) for seismic design and assessment, and of applying prescribed stiffness modifiers with great caution. More refined studies are encouraged.

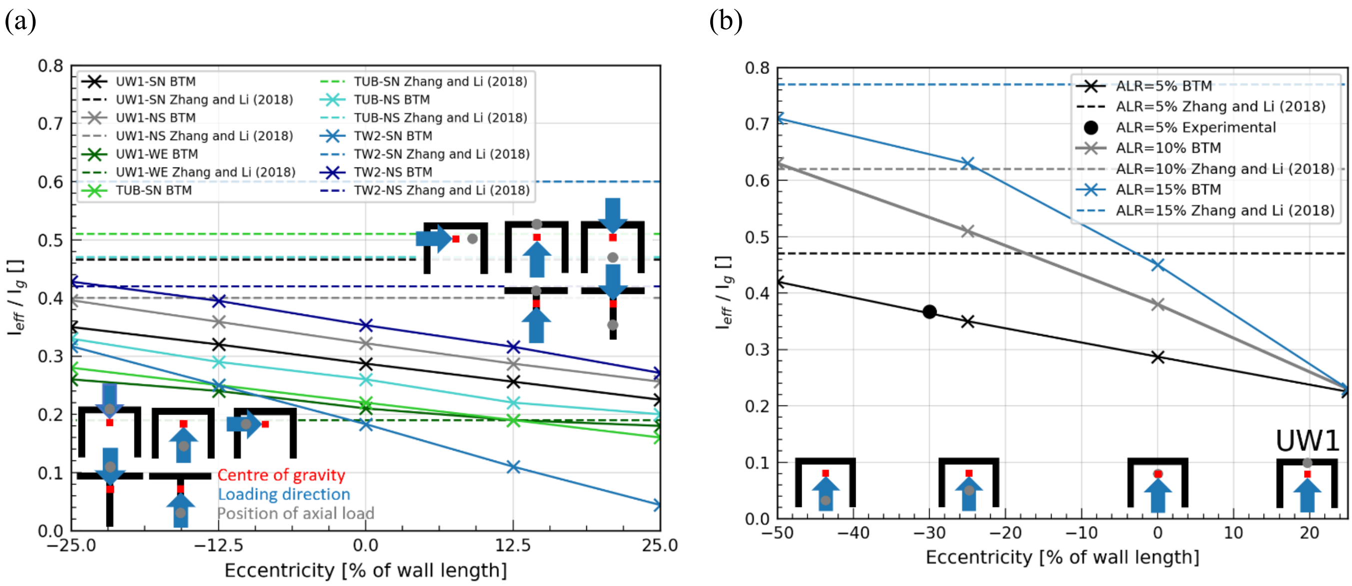

Figure 11. Influence of axial load eccentricity on effective stiffness, as predicted by BTMs and literature expressions, for: (a) units UW1, TW2, and TUB; (b) UW1 with different ALRs, for south-north loading direction.

5.4 *Other Considerations*

The estimation of effective stiffness is an essential step in the process of seismic design, as well as in most assessment procedures, as thoroughly discussed in the Introduction (Section 1). The present sub-section discusses some limitations associated with the computation of effective stiffness as performed in this study, and extends it to address the difficulty in accurate estimations of the effective stiffness more generally.

The wall database considered in this study allowed the computation of 29 experimentally derived effective stiffness datapoints. The latter are obtained from cyclic test results for loading applied along the major or minor section axis, whereas the effective stiffness calculation from BTMs in this study relies on monotonic loading (pushover analyses), as commonly used for nonlinear static analysis. While this was observed to cause only a minor discrepancy for the effective stiffness estimates of most units, it is noted that previous studies using advanced BTMs to simulate both cyclic and monotonic loading (Lu and Panagiotou 2014) have, for certain units, depicted differences between the cyclic loading envelope and pushover results. The latter also tend to predict higher displacement capacities.

The discussion on effective stiffness estimates from cyclic experiments could be extended to non-planar units tested under diagonal loading (Constantin and Beyer 2016; Hoult et al. 2020). The latter were intentionally left out of the assembled database. Diagonal loading is often a complex experimental scenario, usually requiring the simultaneous application of torque to prevent twisting, and the calculation of effective stiffness based on decomposing actuator forces and displacements along two perpendicular axes is questionable. This difficulty can be set within the more general framework of biaxial loading effects on effective stiffness calculation. Whereas monotonic loading is usually a close envelope of the cyclic response of RC units loaded according to common protocols about the same axis, the simultaneous or in-series application of perpendicular displacement components can notably affect their in-plane response. The experimental responses of Wall1, Wall2, and Wall3, discussed in Section 3.4, illustrate this point. Figure 6 (b) shows the stiffness and strength reduction resulting from the application of perpendicular loading phases in Wall3. While the effective stiffness along the south-north direction remained essentially unchanged as it corresponded to the first loading direction subjected to Wall3, the effective stiffness along the north-south direction reduced of 66% when compared to its counterpart Wall2 under uniaxial loading in the same direction. Along the west-east and east-west directions, shown in Figure 6 (a), the reductions of 22% and 68% in effective stiffnesses, with respect to those of uniaxially loaded Wall1, are also consequential.

The aforementioned point underscores the challenges in accurately determining the effective stiffness of walls from biaxial cyclic responses, a complexity that intensifies when considering RC walls in real structures exposed to strong ground motions. In such conditions, these elements experience multi-axial dynamic excitations, together with frame effects from adjoining coupling beams,

beams, or slabs, not to mention higher-order mode effects, all of which are bound to influence a proxy wall effective stiffness value for design and assessment. Possibly, a broader consideration of these effects could lead to new proposals to improve the definition of non-planar wall effective stiffness. In particular, the investigation of the effective stiffness of non-planar coupled walls appears to be of special interest, as both axial load ratio variation and eccentricity would need to be explicitly accounted for.

6 Conclusions

The effective stiffness of members in reinforced concrete buildings is a critical parameter in force-based (FB) seismic design and assessment, using elastic models, to compute member demands and their required strength, as well as displacements. Inaccurate estimates also contribute to notable discrepancies with respect to the outcome of alternative and more recent displacement-based (DB) approaches. This study focuses on the effective stiffness of non-planar walls, which correspond to the cross-sectional shape of most building core walls, contributing to cover a gap in the literature that essentially addresses rectangular sections.

The work started by assembling a database of experimental cyclic tests on non-planar walls (U-shaped, barbell-shaped, T-shaped, and I-shaped) and determining, from those tests, the corresponding effective stiffnesses. The experimental effective stiffness ratios for those tested walls ranged between 6% and 37.5%, with an average of 18.6%. Those values were observed to substantially vary with the cross-section geometry, loading axis, and direction of load application. Current design code expressions do not account for the previous parameters, leading to variable but generally significant overestimations of the effective stiffness of non-planar walls. This has important implications for force-based design approaches, leading to artificially large seismic design force demands and unconservative displacement and drift demands, incompatible with more accurate DB approaches. Whilst specific expressions in the literature for non-planar walls offer some improvement, they remain imprecise and overall quite conservative. The average relative difference between effective stiffness proposals in the literature and codes, with respect to experimentally derived values, ranges from approximately 50% to 200%.

Pushover analyses of the walls in the database were subsequently conducted using a simplified, standardised, numerically stable, and computationally efficient version of a leading state-of-the-art model, the nonlinear beam-truss model (BTM). In general, the BTMs provided a satisfactory agreement with the units' cyclic response envelope along both uniaxial directions. Featuring a small computational cost, BTMs are hence a desirable practical tool for modelling non-planar walls in engineering practice, namely for nonlinear static analyses of RC buildings in the context of DB design and assessment. Alternatively, and perhaps more importantly, since the BTM yielded results closely matching the experimentally derived effective stiffnesses, it can serve as a practical tool to estimate the effective-to-gross moment of inertia for any slender code-designed non-planar wall geometry under a given axial load ratio and eccentricity.

This investigation showed that the two widely used methods for estimating effective stiffness yield comparable results for non-planar sections, except for high axial load ratios. Additionally, the study underscored the significant impact of the axial load ratio on the effective stiffness and examined for the first time the effect of axial load eccentricity relative to the wall section's centre of gravity. The findings indicate that an eccentricity in the opposite direction of the applied lateral load can considerably enhance the effective stiffness of the wall, and conversely, highlighting the importance of precisely determining the location of axial load application due to gravity loads. Finally, the study also emphasized how the in-plane cyclic response of experimentally tested non-planar walls is affected by displacements applied in the perpendicular direction, an effect also accurately modelled by the BTM. The role of biaxial loading in the calculation of effective stiffness suggests the need for potential revisions to its definition. In view of its significance for seismic design, it is anticipated that this study will encourage further investigations on the effective stiffness of non-planar walls including the abovementioned parameters.

Given the strong dependence of effective stiffness on cross-sectional configuration, loading direction, axial load ratio, and axial load eccentricity, the authors recommend the development of a dedicated BTM, or another validated model, as a necessary preliminary step for estimating the effective stiffness of specific non-planar RC walls to be assigned to linear-elastic models for FB design and assessment.

Declaration of Competing Interest

The authors declare that they have no known competing financial interests or personal relationships that could have appeared to influence the work reported in this paper.

Acknowledgments

The authors would like to express sincere gratitude to Mathis Keirle and Christophe Saegerman for their contributions to this research.

Disclosure Statement

No potential conflicts of interest are reported by the authors.

7 References

Adebar, P., and E. Dezhdar. 2015. "Effective stiffness for linear dynamic analysis of concrete shear wall buildings: CSA A23.3-2014." *The 11th Canadian Conference on Earthquake Engineering*.

Adebar, P., A. M. M. Ibrahim, and M. Bryson. 2007. "Test of high-rise core wall: Effective stiffness for seismic analysis." *ACI Struct J*, 104 (5): 549–559.

Almeida, J. P. de, S. De Visscher, H. Varum, and A. A. Correia. 2022. "Harmonising force-based and displacement-based design approaches for the next generation of Eurocode 8: Application to reinforced concrete moment resisting frames." *Eng Struct*, 272.

Almeida, J. P., R. Hoult, A. Bertholet, P. Candeias, A. Carvalho, A. A. Correia, C. Doneux, C. Gwendal, Y. Han, T. Isakovic, A. Janevski, S. Lo Feudo, B. Mihaylov, A. Orgnoni, B. Payen, D. Palermo, R. Pinho, F. Ribeiro, A. Simar, and M. L. Sousa. 2024. "Shake-table testing of two U-shaped RC walls: Overview of the project ERIES-ALL4wALL." *18th World Conference of Earthquake Engineering (WCEE2024)*.

Almeida, J. P., O. Prodan, A. Rosso, and K. Beyer. 2017. "Tests on thin reinforced concrete walls subjected to in-plane and out-of-plane cyclic loading." *Earthquake Spectra*, 33 (1): 323–345. https://doi.org/10.6084/m9.figshare.3490754.v2.

Almeida, J. P., D. Tarquini, and K. Beyer. 2016. "Modelling approaches for inelastic behaviour of RC walls: multi-level assessment and dependability of results." *Archives of Computational Methods in Engineering*, 23 (1): 69–100. https://doi.org/10.1007/s11831-014-9131-y.

Álvarez, R., J. I. Restrepo, and M. Panagiotou. 2020. "RC Wall Plastic Hinge Out-of-Plane Buckling: Analysis Using the Nonlinear Beam-Truss Model." *Journal of Structural Engineering*, 146 (12). American Society of Civil Engineers (ASCE). https://doi.org/10.1061/(asce)st.1943-541x.0002836.

Alvarez, R., J. I. Restrepo, M. Panagiotou, and A. R. Santhakumar. 2019. "Nonlinear cyclic Truss Model for analysis of reinforced concrete coupled structural walls." *Bulletin of Earthquake Engineering*, 17 (12): 6419–6436. Springer Netherlands. https://doi.org/10.1007/s10518-019-00639-8.

American Concrete Institute. 2019. *318-19 Building Code Requirements for Structural Concrete and Commentary*. *318-19 Building Code Requirements for Structural Concrete and Commentary*. American Concrete Institute.

American Society of Civil Engineers. 2017. *ASCE/SEI 41-17: Seismic Evaluation and Retrofit of Existing Buildings*. Reston, VA: American Society of Civil Engineers.

Arteta, C. A., G. A. Araújo, A. M. Torregroza, A. F. Martínez, and Y. Lu. 2019. "Hybrid approach for simulating shear–flexure interaction in RC walls with nonlinear truss and fiber models." *Bulletin of Earthquake Engineering*, 17 (12): 6437–6462. Springer Netherlands. https://doi.org/10.1007/s10518-019-00681-6.

Aydin, B. B., K. Tuncay, and B. Binici. 2019. "Simulation of reinforced concrete member response using lattice model." *Journal of Structural Engineering*, 145 (9). American Society of Civil Engineers (ASCE). https://doi.org/10.1061/(asce)st.1943-541x.0002381.

Beyer, K., A. Dazio, and M. J. N. Priestley. 2008a. "Inelastic wide-column models for U-shaped reinforced concrete walls." *Journal of Earthquake Engineering*, 12 (SUPPL. 1): 1–33. https://doi.org/10.1080/13632460801922571.

Beyer, K., A. Dazio, and M. J. N. Priestley. 2008b. "Quasi-static cyclic tests of two U-shaped reinforced concrete walls." *Journal of Earthquake Engineering*, 12 (7): 1023–1053. https://doi.org/10.1080/13632460802003272.

Brueggen, B. L. 2009. "Performance of T-shaped reinforced concrete structural walls under multi-directional loading." *PhD Thesis, University of Minnesota*.

Brueggen, B. L., C. E. French, and S. Sritharan. 2017. "T-Shaped RC Structural Walls Subjected to Multidirectional Loading: Test Results and Design Recommendations." *Journal of Structural Engineering*, 143 (7). American Society of Civil Engineers (ASCE). https://doi.org/10.1061/(asce)st.1943-541x.0001719.

Burgos, E. A., R. D. Lequesne, and A. Lepage. 2024. *Earthquake-resistant T-shaped concrete walls with high-strength steel bars (SM Report No. 142)*.

Calabrese, A., J. P. Almeida, and R. Pinho. 2010. "Numerical issues in distributed inelasticity modeling of RC frame elements for seismic analysis." *Journal of Earthquake Engineering*, 14 (S1): 38–68. https://doi.org/10.1080/13632469.2010.495681.

Carrillo, J., E. Cubillos, and P. F. Parra. 2022. "Modeling the seismic response of thin concrete walls using the non-linear Beam-Truss Model." *Journal of Building Engineering*, 52. Elsevier Ltd. https://doi.org/10.1016/j.jobe.2022.104424.

CEN (European Committee for Standardization). 2004a. *EN 1998-1:2004 Eurocode 8 — Design of structures for earthquake resistance - Part 1: General rules, seismic actions and rules for buildings*. techreport. Brussels.

CEN (European Committee for Standardization). 2004b. *EN 1992-1-1:Eurocode 2: Design of concrete structures - Part 1-1: General rules and rules for buildings*.

CEN (European Committee for Standardization). 2024. *EN 1998-1-1:2024 Eurocode 8 – Design of structures for earthquake resistance – Part 1-1: General rules and seismic action*.

Computers and Structures Inc. 2018. "User guide PERFORM-3D: Nonlinear analysis and performance assessment for 3D-Version 7." USA.

Constantin, R., and K. Beyer. 2016. "Behaviour of U-shaped RC walls under quasi-static cyclic diagonal loading." *Eng Struct*, 106 (1): 36–52. Elsevier Ltd. https://doi.org/10.1016/j.engstruct.2015.10.018.

Correia, A. A., J. P. Almeida, and R. Pinho. 2015. "Force-based higher-order beam element with flexural-shear-torsional interaction in 3D frames. Part I: Theory." *Eng Struct*, 89: 204–217. Elsevier Ltd. https://doi.org/10.1016/j.engstruct.2014.10.024.

Dameh, F., and S. J. Pantazopoulou. 2024. "Strain penetration effects on lateral strength and deformation capacity of U-shaped walls." *Bulletin of Earthquake Engineering*. Springer Science and Business Media B.V. https://doi.org/10.1007/s10518-024-02060-2.

Das, S., and S. Choudhury. 2019. "Influence of effective stiffness on the performance of RC frame buildings designed using displacement-based method and evaluation of column effective stiffness using ANN." *Eng Struct*, 197. Elsevier Ltd. https://doi.org/10.1016/j.engstruct.2019.109354.

Deng, X., I. Koutromanos, J. Murcia-Delso, and M. Panagiotou. 2021. "Nonlinear truss models for strain-based seismic evaluation of planar RC walls." *Earthq Eng Struct Dyn*, 50 (11): 2939–2960. John Wiley and Sons Ltd. https://doi.org/10.1002/eqe.3480.

Fenwick, R., and D. Bull. 2000. "What is the stiffness of reinforced concrete walls?" *SESOC Journal*, 13 (2): 23–32.

Feron, J., P. Latteur, and J. Pacheco de Almeida. 2024. "Static modal analysis: A review of static structural analysis methods through a new modal paradigm." *Archives of Computational Methods in Engineering*, 31 (6): 3409–3440. Springer Science and Business Media B.V. https://doi.org/10.1007/s11831-024-10082-x.

Fischinger, M., T. Isakovic, and P. Kante. 2004. "Implementation of a macro model to predict seismic response of RC structural walls." *Computers and Concrete*, 1 (2): 211–226. Techno-Press. https://doi.org/10.12989/cac.2004.1.2.211.

Girgin, S. C., I. Koutromanos, and M. Moharrami. 2016. “Numerical Simulation of Reinforced Concrete Members with Reinforcing Bar Buckling.” *12th International Congress on Advances in Civil Engineering*.

Godinez, S., R. Alvarez, and J. Restrepo. 2024. “Nonlinear dynamic seismic analysis of a high-rise concrete core wall building with podiums using the beam-truss model.” *Bulletin of Earthquake Engineering*.

Hoult, R., and J. P. Almeida. 2024. “Modified compression field theory and disturbed stress field model on the simulation of the global and local behaviour of non-planar reinforced concrete walls under cyclic and dynamic loading.” *Bulletin of Earthquake Engineering*. Springer Science and Business Media B.V. https://doi.org/10.1007/s10518-024-01982-1.

Hoult, R., A. Appelle, J. Almeida, and K. Beyer. 2020. “Seismic performance of slender RC U-shaped walls with a single-layer of reinforcement.” *Eng Struct*, 225. Elsevier Ltd. https://doi.org/10.1016/j.engstruct.2020.111257.

Hoult, R., A. Bertholet, and J. P. de Almeida. 2023a. “Core versus Surface Sensors for Reinforced Concrete Structures: A Comparison of Fiber-Optic Strain Sensing to Conventional Instrumentation.” *Sensors*, 23 (3). MDPI. https://doi.org/10.3390/s23031745.

Hoult, R., A. A. Correia, and J. P. de Almeida. 2023b. “Beam-Truss Models to Simulate the Axial-Flexural-Torsional Performance of RC U-Shaped Wall Buildings.” *CivilEng*, 4 (1): 292–310. MDPI. https://doi.org/10.3390/civileng4010017.

Hoult, R., C. Doneux, and J. Pacheco de Almeida. 2023c. “Tests on reinforced concrete U-shaped walls subjected to torsion and flexure.” *Earthquake Spectra*, 39 (4): 2685–2710. SAGE Publications Inc. https://doi.org/10.1177/87552930231195315.

Ile, N., and J. M. Reynouard. 2005. “Behaviour of U-shaped walls subjected to uniaxial and biaxial cyclic lateral loading.” *Journal of Earthquake Engineering*, 9 (1): 67–94.

Isaković, T., and M. Fischinger. 2019. “Assessment of a force–displacement based multiple-vertical-line element to simulate the non-linear axial–shear–flexure interaction behaviour of reinforced concrete walls.” *Bulletin of Earthquake Engineering*, 17 (12): 6369–6389. Springer Netherlands. https://doi.org/10.1007/s10518-019-00680-7.

Janevski, A., and T. Isaković. 2024. “Blind prediction and post-experimental analysis of RC core wall’s cyclic flexural response using MVLEM-FD.” *Bulletin of Earthquake Engineering*.

Kabeyasawa, T., H. Shiohara, S. Otani, and H. Aoyama. 1983. “Analysis of the Full-Scale Seven-Story Reinforced Concrete Test Structure.” *Journal of the Faculty of Engineering, The University of Tokyo*, 37 (2): 431–478.

Kazaz, İ. 2024. “Evaluation of shear wall design and practice after the 6 February 2023 Kahramanmaraş earthquakes.” *18th World Conference of Earthquake Engineering (WCEE2024)*.

Kolozvari, K., C. Arteta, M. Fischinger, S. Gavridou, M. Hube, T. Isaković, L. Lowes, K. Orakcal, J. Vásquez, and J. Wallace. 2018. “Comparative study of state-of-the-art macroscopic models for planar reinforced concrete walls.” *ACI Struct J*, 115 (6): 1637–1657. American Concrete Institute. https://doi.org/10.14359/51710835.

Kolozvari, K., C. N. López, and L. M. Massone. 2023. “Efficient three-dimensional shear-flexure interaction model for reinforced concrete walls.” *Eng Struct*, 294. Elsevier Ltd. https://doi.org/10.1016/j.engstruct.2023.116700.

Li, B., and W. Xiang. 2011. “Effective Stiffness of Squat Structural Walls.” *Journal of Structural Engineering*, 137 (12): 1470–1479. American Society of Civil Engineers (ASCE). https://doi.org/10.1061/(asce)st.1943-541x.0000386.

Lu, Y., and M. Panagiotou. 2012. *Report No. UCB/SEMM-2012/01: Three-dimensional nonlinear cyclic beam-truss model for non-planar reinforced concrete walls*. Berkeley.

Lu, Y., and M. Panagiotou. 2014. “Three-dimensional cyclic beam-truss model for nonplanar reinforced concrete walls.” *Journal of Structural Engineering*, 140 (3). American Society of Civil Engineers (ASCE). https://doi.org/10.1061/(asce)st.1943-541x.0000852.

Lu, Y., M. Panagiotou, and I. Koutromanos. 2014. *PEER Report 2014/18: Three-Dimensional Beam-Truss Model for Reinforced-Concrete Walls and Slabs Subjected to Cyclic Static or Dynamic Loading*.

Lu, Y., M. Panagiotou, and I. Koutromanos. 2016. “Three-dimensional beam-truss model for reinforced concrete walls and slabs – part 1: modeling approach, validation, and parametric study for individual reinforced concrete walls.” *Earthq Eng Struct Dyn*, 45 (9): 1495–1513. John Wiley and Sons Ltd. https://doi.org/10.1002/eqe.2719.

Ma, J., and B. Li. 2018. “Experimental and analytical studies on h-shaped reinforced concrete squat walls.” *ACI Struct J*, 115 (2): 425–438. American Concrete Institute. https://doi.org/10.14359/51701144.

Ma, J., and B. Li. 2019. “Seismic Behavior of L-Shaped RC Squat Walls under Various Lateral Loading Directions.” *Journal of Earthquake Engineering*, 23 (3): 422–443. Taylor and Francis Ltd. https://doi.org/10.1080/13632469.2017.1326424.

Ma, J., Z. Zhang, and B. Li. 2018. “Experimental assessment of T-shaped Reinforced concrete squat walls.” *ACI Struct J*, 115 (3): 621–634. American Concrete Institute. https://doi.org/10.14359/51701294.

Mander, J. B., M. J. N. Priestley, and R. Park. 1988. “Theoretical stress-strain model for confined concrete.” *Journal of Structural Engineering*, 114 (8): 1804–1825.

Mavros, M., J. Murcia-Delso, M. Panagiotou, and I. Koutromanos. 2026. “Blind-prediction analysis of reinforced concrete U-shaped walls under flexural or torsional loading using the BTM-shell method.” *Bulletin of Earthquake Engineering*, 24:179-210.

Mavros, M., M. Panagiotou, I. Koutromanos, R. Alvarez, and J. I. Restrepo. 2022. “Seismic analysis of a modern 14-story reinforced concrete core wall building system using the BTM-shell methodology.” *Earthq Eng Struct Dyn*, 51 (6): 1540–1562. John Wiley and Sons Ltd. https://doi.org/10.1002/eqe.3627.

Mavros, M., M. Panagiotou, I. Koutromanos, and J. I. Restrepo. 2023. “Nonlinear dynamic seismic analysis of a modern concrete core wall building in Los Angeles using the BTM-shell methodology.” *Earthq Eng Struct Dyn*, 52 (14): 4416–4441. John Wiley and Sons Ltd. https://doi.org/10.1002/eqe.3956.

McKenna, F. 2011. “OpenSees: a framework for earthquake engineering simulation.” *Comput Sci Eng*, 13 (4): 58–66.

Menegotto, M., and P. Pinto. 1973. “Method of analysis for cyclically loaded R.C. plane frames including changes in geometry and non-elastic behavior of elements under combined normal force and bending.” *Proc. of the Symposium Resistance and Ultimate Deformability of Structures Loads, Acted on by Well-Defined Repeated*. Lisbon, Portugal.

Mestyanek, J. M. 1986. “The earthquake resistance of reinforced concrete structural walls of limited ductility.” Christchurch, New Zealand: University of Canterbury.

Miki, T., and J. Niwa. 2004. “Nonlinear analysis of RC structural members using 3D lattice model.” *Journal of Advanced Concrete Technology*, 2 (3): 343–358. https://doi.org/10.3151/jact.2.343.

Mohammed, M. A., and A. R. Barbosa. 2019. “Numerical modeling strategy for the simulation of nonlinear response of slender reinforced concrete structural walls.” *CMES - Computer Modeling in Engineering and Sciences*, 120 (3): 583–627. Tech Science Press. https://doi.org/10.32604/cmes.2019.06052.

Murcia-Delso, J., I. Koutromanos, X. Deng, P. Luna, M. Panagiotou, and N. Duarte. 2024. “New framework for seismic evaluation of RC wall structures based on simulation and material strains.” *18th World Conference on Earthquake Engineering - WCEE2024*.

New Zealand Standard. 2006. *Concrete structures standard NZS 3101:Part 1:2006*. Standards New Zealand.

National Institute of Standards and Technology. 2017. *NIST GCR 17-917-45: Recommended modeling parameters and acceptance criteria for nonlinear analysis in support of seismic evaluation, retrofit, and design*. Gaithersburg, MD.

Oesterle, R. G., A. E. Fiorato, L. S. Johal, J. E. Carpenter, H. G. Russell, and W. G. Corley. 1976. "Earthquake resistant structural walls - Tests of isolated walls." *Research and Development Construction Technology Laboratories, Portland Cement Association*.

Orakcal, K., L. M. Massone, and J. W. Wallace. 2006. *Analytical Modeling of Reinforced Concrete Walls for Predicting Flexural and Coupled Shear-Flexural Responses*. *Pacific Earthquake Engineering Research Center*. Los Angeles, California.

Orgnoni, A., and R. Pinho. 2024. "Applied Element Modelling of Cyclic Flexural and Torsional Response of Non-Planar RC Walls." *Bulletin of Earthquake Engineering*.

Paulay, T., and M. J. N. Priestley. 1992. *Seismic Design of Reinforced Concrete and Masonry Buildings*. *John Wiley & Sons*.

Priestley, M. J. N., G. M. Calvi, and M. J. Kowalsky. 2007. *Displacement-based Seismic Design of Structures*. *IUSS Press*.

Rahimian, A. 2011. "Lateral stiffness of concrete shear walls for tall buildings." *ACI Struct J*, 108 (6): 755–765.

Samanta, N., and & K. Dasgupta. 2024. "Improving the seismic behaviour of flanged slender RC structural wall using enlarged boundary element." *18th World Conference on Earthquake Engineering (WCEE2024)*.

SeismoSoft. 2023. "SeismoStruct 2023 - A Computer Program for Static and Dynamic Nonlinear Analysis of Framed Structures, available from http://www.seismosoft.com."

Sharifi, M., and M. Shafieian. 2018. "Effective stiffness of concrete shear walls based on statistical analysis." *Structural Concrete*, 19 (6): 1560–1576. Wiley-Blackwell. https://doi.org/10.1002/suco.201600202.

Suquillo, B., F. Rojas, C. López, and L. Massone. 2026. "MEFI 3D: A membrane fiber element for non-planar reinforced concrete structural walls." *Bulletin of Earthquake Engineering*, 24:211-238.

Tarquini, D., J. P. de Almeida, and K. Beyer. 2019. "Experimental investigation on the deformation capacity of lap splices under cyclic loading." *Bulletin of Earthquake Engineering*, 17 (12): 6645–6670. Springer Netherlands. https://doi.org/10.1007/s10518-019-00692-3.

Tastani, S. P., and S. J. Pantazopoulou. 2015. "Implications of yield penetration on confinement requirements of RC wall elements." *Earthquakes and Structures*, 9 (4): 831–849.

Thomsen IV, J. H., and J. W. Wallace. 1995. “Displacement—Based Design of Reinforced Concrete Structural Walls: An Experimental Investigation of Walls with Rectangular and T-Shaped Cross-Sections.” *Nsf*.

Tura, C., K. Orakcal, M. F. Gullu, and A. Ilki. 2026. “A new layered shell model for reinforced concrete walls I: Model description and dynamic response simulations.” *Bulletin of Earthquake Engineering*, 24:43-92.

Vulcano, A., V. V. Bertero, and V. Colotti. 1988. “Analytical modeling or R/C structural walls.” *9th World Conference of Earthquake Engineering*. Tokyo, Japan.

Vuran, E., C. Serhatoğlu, M. Ö. Timurağaoğlu, E. Smyrou, İ. E. Bal, and R. Livaoğlu. 2024. “Damage observations of RC buildings from 2023 Kahramanmaraş earthquake sequence and discussion on the seismic code regulations.” *Bulletin of Earthquake Engineering*, (February 2023). https://doi.org/10.1007/s10518-023-01843-3.

Wibowo, A., J. L. Wilson, N. T. K. Lam, and E. F. Gad. 2013. “Seismic performance of lightly reinforced structural walls for design purposes.” *Magazine of Concrete Research*, 65 (13): 809–828. https://doi.org/10.1680/macr.13.00021.

Wong, J.-M., A. Sommer, K. Briggs, and C. Ergin. 2017. “Effective stiffness for modeling reinforced concrete structures: A literature review.” *Structure Magazine*, 18–21.

Zhang, P., J. I. Restrepo, J. P. Conte, and J. Ou. 2017. “Nonlinear finite element modeling and response analysis of the collapsed Alto Rio building in the 2010 Chile Maule earthquake.” *Structural Design of Tall and Special Buildings*. John Wiley and Sons Ltd.

Zhang, Z., and B. Li. 2018. “Effective Stiffness of Non-Rectangular Reinforced Concrete Structural Walls.” *Journal of Earthquake Engineering*, 22 (3): 382–403. Taylor and Francis Ltd. https://doi.org/10.1080/13632469.2016.1224744.